PHYSICAL REVIEW D

PARTICLES AND FIELDS

THIRD SERIES, VOLUME 37, NUMBER 7 1 APRIL 1988

Charm production in nonresonant e^+e^- annihilations at $\sqrt{s} = 10.55$ GeV

D. Bortoletto, M. Goldberg, R. Holmes, N. Horwitz, A. Jawahery, P. Lubrano, G. C. Moneti, V. Sharma, I. P. J. Shipsey, and P. Thoma
Syracuse University, Syracuse, New York 13244

S. E. Csorna, T. Letson, M. D. Mestayer, R. S. Panvini, and G. B. Word
Vanderbilt University, Nashville, Tennessee 37235

A. Bean, G. J. Bobbink, I. C. Brock, T. Ferguson, R. W. Kraemer, and H. Vogel
Carnegie Mellon University, Pittsburgh, Pennsylvania 15213

C. Bebek, K. Berkelman, E. Blucher, D. G. Cassel, T. Copie, R. DeSalvo, J. W. DeWire, R. Ehrlich, R. S. Galik, M. G. D. Gilchriese, B. Gittelman, S. W. Gray, A. M. Halling, D. L. Hartill, B. K. Heltsley, S. Holzner, J. Kandaswamy, R. Kowalewski, D. L. Kreinick, Y. Kubota, N. B. Mistry, J. Mueller, R. Namjoshi, E. Nordberg, D. Perticone, D. Peterson, M. Pisharody, K. Read, D. Riley, A. Silverman, and S. Stone
Cornell University, Ithaca, New York 14853

A. J. Sadoff
Ithaca College, Ithaca, New York 14850

P. Avery, D. Besson, and L. Garren
University of Florida, Gainesville, Florida 32611

T. Bowcock, K. Kinoshita, F. M. Pipkin, M. Procario, Richard Wilson, J. Wolinski, and D. Xiao
Harvard University, Cambridge, Massachusetts 02138

P. Haas, M. Hempstead, T. Jensen, D. R. Johnson, H. Kagan, and R. Kass
Ohio State University, Columbus, Ohio 43210

P. Baringer, R. L. McIlwain, D. H. Miller, and E. I. Shibata
Purdue University, West Lafayette, Indiana 47907

S. Behrends, Jan M. Guida, Joan A. Guida, F. Morrow, R. Poling, E. H. Thorndike, and P. Tipton
University of Rochester, Rochester, New York 14627

M. S. Alam, N. Katayama, I. J. Kim, W. C. Li, X. C. Lou, C. R. Sun, and V. Tanikella
State University of New York at Albany, Albany, New York 12222
(Received 26 October 1987)

We report results on the differential and total cross sections for inclusive production of the charmed particles D^{*+}, D^{*0}, D^0, D^+, D_s, and Λ_c in e^+e^- annihilations at $\sqrt{s} = 10.55$ GeV. Widely used quark fragmentation models are discussed and compared with the measured charmed-particle momentum distributions. This comparison, as well as that with measurements at other center-of-mass energies, shows the need to take QCD corrections into account and their importance

for a correct interpretation of the model parameters. The observed rate of D^0 and D^+ production is compared to the expected total charm production cross section. We measure the probability of a charmed meson being produced as a vector meson and the D^{*+} decay branching fraction into $D^0\pi^+$.

I. INTRODUCTION

The production of charmed particles in nonresonant e^+e^- annihilation is interesting for various reasons. The total cross section for $e^+e^-\to c\bar{c}$ is simply predicted by QED with some QCD corrections;[1] and this prediction is supported by the observed change[2] in the total cross section for hadron production when passing the threshold for charm production. Since each $e^+e^-\to c\bar{c}$ annihilation produces one and only one charmed-particle–antiparticle pair, this prediction can easily be compared with the sum of the observed cross sections for charmed-particle production. Of further interest is the determination of the relative proportions in the charmed-particle sector of mesons and baryons, of vector and pseudoscalar mesons, and of nonstrange and strange mesons.

The hadronization process through which quarks and gluons transform themselves into a jet of hadrons is still poorly understood. Quantum chromodynamics (QCD) is believed by most to be the correct theory of the interaction between quarks and gluons, but reliable calculations are possible only in the perturbative regime ($\alpha_s \ll 1$). The hadronization process seems to be dominated by the color-confining forces ($\alpha_s > 1$), and its experimental study is thus of great importance in providing guidance to the development of suitable nonperturbative QCD computational methods. At present the description of hadronization relies, at one stage or another, on educated modeling.[3–8]

Some basic characteristics of hadron jets, mainly their collimation and particle multiplicity, have been known for a long time.[9] A more detailed description is provided by the fragmentation functions $D_q^h(v)$, defined as the (unnormalized) probability density for a jet initiated by a quark q to generate a hadron of type h with a fraction v of the initial-quark four-momentum.

In most cases the light hadrons in a jet have as constituents the light quarks produced in the fragmentation of the color string, and only rarely do they contain the primary quark. Their differential production cross section is related to the fragmentation functions of all the quarks through a set of complex equations and it is not easy to extract from the data the complete set of fragmentation functions.

The situation is very different in the case of hadrons containing charm or heavier flavors. If we believe that the generation of quark-antiquark pairs in the fragmentation process is a tunneling effect, it follows that the probability of extracting from the vacuum a charm-anticharm pair (or heavier) is exceedingly small. This means that heavy-flavored particles necessarily contain the primary quark, and thus their differential cross section is simply proportional to the relevant fragmentation function.

Electron-positron annihilations well above charm threshold are an abundant source of nearly monochromatic charm quarks, and are thus well suited to the study of the charm fragmentation functions of the various charmed mesons and baryons. Charm fragmentation has been studied at the SLAC storage ring PEP (Refs. 10–15) and at the DESY storage rings PETRA (Refs. 16–19) and DORIS (Refs. 20–22). At the Cornell Electron Storage Ring (CESR), the CLEO Collaboration has measured the fragmentation function of the charm quark into D^{*+} and D^0 (Ref. 23), D_s (Ref. 24), and Λ_c (Ref. 25). In this paper we report substantially improved results from the CLEO experiment on the fragmentation into D^{*+}, D^0, and D_s, and new results on D^{*0}, D^+, and Λ_c (here, and throughout this paper, charge-conjugate modes are implied). The detection of different decay modes of charmed particles also allows the determination of some of their relative decay branching fractions.

In Sec. II we give a brief description of the relevant characteristics of our detector. In Sec. III we describe the general procedures used to identify charmed particles in our data and to determine their respective detection efficiencies. We present our measured charmed-particle differential and total cross sections in Sec. IV. These results are compared to data at other center-of-mass energies by using an evolution technique which accounts for QCD radiative corrections. From our data we also measure the ratio of two D^0 branching fractions as well as the fraction of the total charm cross section composed of D^0 and D^+ meson production.

Section V reports our measurements of the relative probability of vector to pseudoscalar-charmed-meson production and of the branching ratio $B(D^{*+}\to D^0\pi^+)$. In Sec. VI we review the present understanding of the fragmentation process and describe the various theoretical expressions for the heavy-flavor fragmentation function. We point out the importance of QED and QCD corrections to these theoretical fragmentation functions. We then fit our charmed-particle differential cross sections to the predictions of the Lund symmetric Monte Carlo model including all QED and QCD corrections, as well as directly to various theoretical fragmentation functions. We emphasize the large differences in the values obtained for the theoretical fragmentation parameters using these two techniques. Finally, in Sec. VIII we summarize our results and conclusions.

II. DETECTOR AND EVENT-SELECTION PROCEDURES

The nonresonant charm events were produced at center-of-mass energies on and below the $\Upsilon(4S)$ resonance at CESR, and the data were accumulated with the CLEO detector. The detector, the trigger, and the pro-

cedures to select hadronic events have been described elsewhere[26–28] and will thus be described only briefly here. The central region of the detector contains two cylindrical tracking chambers, a 10-layer precision vertex detector and a 17-layer drift chamber, which operate in a 1.0-T magnetic field provided by a superconducting solenoidal magnet. The drift chamber, using pulse-height measurements in all of its 17 layers, is capable of measuring the specific ionization (dE/dx) with an rms resolution of 10%. Surrounding the coil are eight identical sectors of apparatus used for particle identification. In order of distance from the beam line, each sector consists of a three-layer planar drift chamber, a system of pressurized multiple wire proportional chambers (MWPC's) capable of measuring 117 samples of dE/dx (rms resolution 6%), an array of time-of-flight (TOF) scintillation counters (rms resolution 350 ps) in a single layer, and a 12-radiation-length, 44-layer, lead and proportional-tube shower chamber that covers 47% of the full solid angle. The eight sectors are followed by 0.65 to 1.5 m of iron, and a two-dimensional array of planar drift chambers outside this iron for muon identification. Additional drift chambers are interspersed within the iron to allow identification of lower-momentum muons.

The essential components for the analysis presented here are the central tracking chambers, the pressurized dE/dx counters, the time-of-flight counters and the shower chambers. Charged-particle tracking provided by the central tracking system results in a momentum resolution for the combined system of

$$(\Delta p/p)^2=[0.007(\mathrm{GeV}/c)^{-1}p]^2+(0.006)^2 .$$

Charged-hadron identification is provided over 85% of the 4π solid angle by dE/dx in the main drift chamber, over 46% of it by dE/dx in the pressurized MWPC's and by time of flight from the scintillation counters that cover 47% of 4π. Each device used for hadron identification is calibrated using sets of identified pion, kaon, or proton tracks to obtain the expected signal as a function of momentum. The tracks used in the calibration are selected from clean two-body decay signals. In the decay $K_s^0\to\pi^+\pi^-$ the two-pion tracks are identified by their invariant mass and by requiring separation of the $\pi^+\pi^-$ vertex from the event vertex by at least 5 mm. For protons the decay $\Lambda\to p\pi^-$ is used in the same way, excluding secondary vertices ambiguous with K_S^0's. For charged K's at low momentum we use the decay $\phi\to K^+K^-$ and at higher momenta each device is calibrated using tracks identified simultaneously by the other two devices as K's. The dE/dx distribution for each particle is partitioned into several momentum bins and the signal distribution is fitted to a Gaussian shape. The means and widths thus obtained are then fitted to a smooth function of momentum. The time-of-flight resolution is independent of momentum.

Photon showers in the calorimeter are identified as photons if they are unmatched to inner-drift-chamber tracks and have a measured energy in excess of 100 MeV. The photon energy resolution is determined to be $\sigma(E)/E=20\%/\sqrt{E}$ (E in GeV) by measuring a sample of radiative Bhabha events.

Selection of hadronic events

We accepted hadronic events according to the following criteria.

(1) Each event must have at least three charged tracks found in the drift chamber.

(2) There must be a common event vertex lying within ±5 cm of the center of the interaction region along the beam line and ±2 cm transverse to the beam line.

(3) At least 250 MeV of deposited energy must be detected in the shower detectors.

(4) At least 30% of the center-of-mass energy must be visible as charged and neutral tracks.

The charged-multiplicity cut (1) reduces $\tau^+\tau^-$ background; the common vertex requirement (2) helps to eliminate cosmic rays and beam-gas collisions; the electromagnetic shower energy cut (3) is required to suppress events consisting of beam pipe interactions; the charged-energy requirement (4) removes two-photon collision events. The average acceptance for continuum charm events is about 84% as determined by Monte Carlo simulation.

The data reported here are from a sample of 77.3 pb^{-1} accumulated at the $\Upsilon(4S)$ resonance ($\sqrt{s}=10.58$ GeV) and 35.8 pb^{-1} at a continuum energy below $B\bar{B}$ threshold ($\sqrt{s}=10.52$ GeV). About 30% of the events collected at the $\Upsilon(4S)$ contain $\Upsilon(4S)\to B\bar{B}$; the rest are continuum. This data sample may thus be used for studies of continuum processes provided that the particles under examination are in a momentum region forbidden by $B\bar{B}$ decay kinematics, i.e., where $p>2.57$ GeV/c. After applying the above cuts, 450 000 hadronic events survived of which 90 000 are $\Upsilon(4S)\to B\bar{B}$ events.

III. DESCRIPTION OF ANALYSES

Charmed particles are identified from the following decay modes (inclusion of charge-conjugate states is implied):

$$D^0\to K^-\pi^+ , \tag{1}$$

$$D^+\to K^-\pi^+\pi^+ , \tag{2}$$

$$D^{*+}\to D^0\pi^+ \quad \text{with} \quad D^0\to K^-\pi^+ \tag{3a}$$

$$\text{or} \quad D^0\to K^-\pi^+\pi^-\pi^+ , \tag{3b}$$

$$D^{*0}\to D^0(\gamma \text{ or } \pi^0) \quad \text{with} \quad D^0\to K^-\pi^+ , \tag{4}$$

$$D_s^+\to\phi\pi^+ \quad \text{with} \quad \phi\to K^+K^- , \tag{5}$$

$$\Lambda_c^+\to pK^-\pi^+ . \tag{6}$$

Each of the above particles is identified by the examination of distributions of the invariant mass of combinations of two or more tracks. In order to minimize systematic uncertainties, all analysis procedures have been standardized as much as possible. Track reconstructions which are not consistent with coming from the event vertex are rejected. All track momenta are corrected for ionization energy losses in the beam pipe.

In several cases it is useful to reduce the background from random combinations by requiring that each track pass loose or stringent requirements on particle identification. For particle identification information to be considered valid, we require that the number of hits in the dE/dx chambers and the drift chamber be greater than 60 and 10, respectively. The looser requirement of "consistency" accepts tracks satisfying loose identification criteria but eliminates those positively identified as other particles. For example, a particle is considered to be consistent with the kaon hypothesis if the measured values of dE/dx and time of flight are within three standard deviations (σ) of the expected values in the drift chamber (for dE/dx measurement) and in at least one of the other two detectors. A particle within 2σ of the expected values in the drift chamber is also considered to be consistent with the kaon hypothesis with no further check in the remaining detectors. A particle is considered "positively identified" if its measurements are within 1σ of the expected values and at least 2σ away from any other alternative identification.

Further kinematic requirements, where appropriate, include those on masses of intermediate particles in cascade decays and on decay angles. Decay angular distributions in the rest frame of a parent particle are often significantly different from the same distributions assembled from random combinations of tracks. For example, the decay angular distribution for an unpolarized particle in its center of mass is isotropic. Choosing the direction of motion of the parent in the laboratory frame as the reference axis, the decay angle θ of a daughter particle in the parent's rest frame with respect to this axis is distributed uniformly in $\cos\theta$. Background combinations tend to have distributions peaked in the forward and backward directions, because of the jetlike nature of the continuum events.

We examine each combination of tracks with charges consistent with the final state under consideration. If all of the tracks pass the quality and identification requirements, each track is attributed the appropriate mass and the invariant masses of the combination and any relevant subcombinations are calculated. For those combinations passing further kinematic cuts the appropriate invariant masses are histogrammed in several momentum intervals. The momentum bins are determined by our choice of fragmentation variable. While this will be discussed later in Sec. IV A, we anticipate here the definition

$$x^+ = \frac{(E+p)}{(E+p)_{\max}} , \tag{7}$$

where E and p are the energy and momentum of the hadron and $E_{\max}$ and $p_{\max}$ are their maximum attainable values. For candidates with momenta above the kinematic limit for β decay products ($p > 2.57$ GeV/c or $x^+ > 0.56$), we use the entire data set of 113.1 pb^{-1}, while for those below we use only the continuum data set of 35.8 pb^{-1}.

In almost all cases the mass distributions are fitted with a signal shape of a Gaussian plus a polynomial background. The means and widths of the Gaussian are fixed to values determined by Monte Carlo simulation. These values and the reconstruction efficiencies are determined in a way designed to minimize the effects of fluctuations in the Monte Carlo simulation. First, the Monte Carlo mass distributions are fitted in each momentum interval allowing the means and widths to vary. The measured means and widths are then fitted to a smooth function of momentum to determine the values with which the data are fit. The mass distributions from the Monte Carlo simulations are then refitted using the fixed mean and width. The efficiencies obtained from this procedure are then smoothed by fitting the measured values to a smooth function of momentum.

We now discuss specific approaches unique to each particle.

A. D^0

For all D^0 candidates we demand $-0.85 < \cos\theta_K < +0.90$, where θ_K is the decay angle of the K^- as defined above. The $K^-\pi^+$ invariant-mass distributions are shown in Fig. 1. Whenever feasible, we show separately the low-momentum mass distribution, where we can use only the continuum annihilation data sample

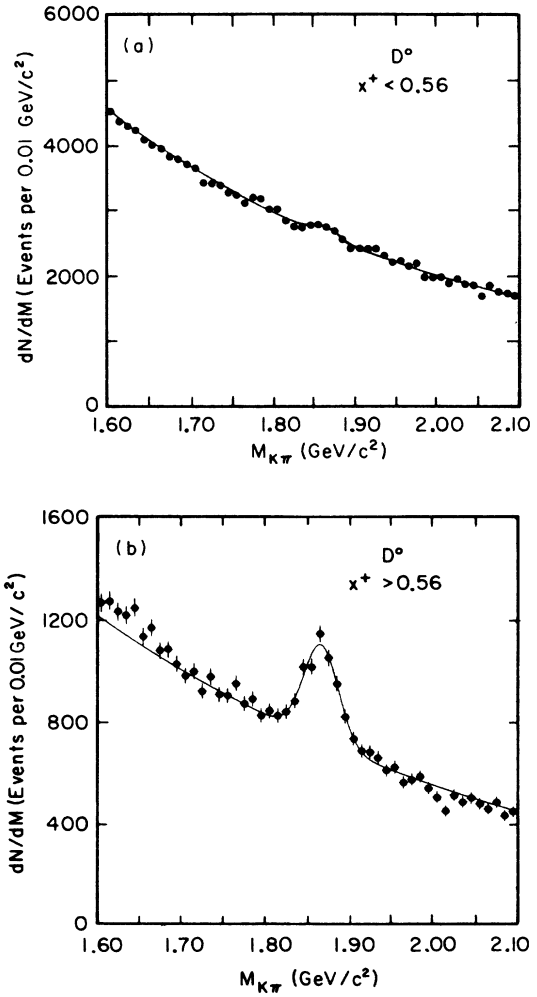

FIG. 1. The $K^-\pi^+$ invariant-mass distribution for (a) $x^+ < 0.56$ and (b) $x^+ > 0.56$ showing the fit to the D^0 peak.

to avoid contamination from B decay products, and the high-momentum mass distribution where we use the full data sample.

Besides the combinatorial background, parametrized by a polynomial, we have in this case also a background due to D^0 decays into $K^-\pi^+$ when the particle-mass assignments are interchanged. The shape of this background has been determined both by direct kinematical calculation and by Monte Carlo simulation. We have parametrized the shape with a rising exponential below the D^0 mass and a falling one above the D^0 mass; the two exponentials are constrained to intersect at the D^0 mass The total area under the two exponentials was constrained to equal the area of the Gaussian that fits the right mass combinations. Since the available particle-identification information has little effect in reducing this background and would only introduce additional uncertainty in the calculated efficiency, we have not used it. Ignoring this effect would lead to overestimating the D^0-production cross section by about 20% in the region $0.5 < x^+ < 0.9$.

We have also considered the effect of the background due to misinterpreted $D^0 \to K^+K^-$ decays. The signal obtained when this is added to the other backgrounds differs from the one obtained disregarding it by a small fraction of the statistical error with a sign that varies randomly from one momentum interval to the other. We have therefore disregarded this effect.

B. D^+

In $D^+ \to K^-\pi^+\pi^+$ decay the K^- candidate is required to have particle identification information consistent with the K^- hypothesis. The $K^-\pi^+\pi^+$ invariant-mass distributions are shown in Fig. 2.

C. D^{*+}

We detect the D^{*+} through its decay into $D^0\pi^+$. Since our efficiency for detecting pions vanishing for pion momenta below about 70 MeV/c, we confine our direct measurement of D^{*+} to D^{*+} momenta greater than 1.0 GeV/c. We found it unnecessary to use particle identification. To increase the signal-to-background ratio, particularly in the low-D^{*+}-momentum bins, we require $\cos\theta_K > -0.80$, where θ_K is the decay angle (as defined above) of the K^- in the D^0 rest frame.

To identify D^{*+}'s we first select those track combinations for which the absolute value of the mass difference $\Delta M = M(\text{“}D^0\text{”}\pi^+) - M(\text{“}D^0\text{”})$ is within 1.5 MeV of the known $D^{*+} - D^0$ mass difference (145.4 MeV). Here “D^0” is an appropriate $K^-\pi^+$ or $K^-\pi^+\pi^-\pi^+$ track combination with an effective mass in the interval 1.40–2.2 GeV. The mass distribution of the D^0 thus selected is then fitted to a Gaussian signal plus background. In the decay $D^{*+} \to (K^-\pi^+\pi^-\pi^+)\pi^+$, the exchange of the K^- and π^- interpretations results in a broad peak in the D^0 candidate mass distribution, which is easily incorporated in the combinatorial background. This would not happen using the inverse procedure: if we were first to select a D^0 candidate, then the candidates with interchanged mass interpretations would obviously contribute a peak in the ΔM distribution of the same width as the signal and would thus be indistinguishable from it. The $K^-\pi^+$ and $K^-\pi^+\pi^-\pi^+$ invariant-mass distributions after the mass-difference selection are shown in Fig. 3.

Although the efficiency for detecting a D^{*+} vanishes

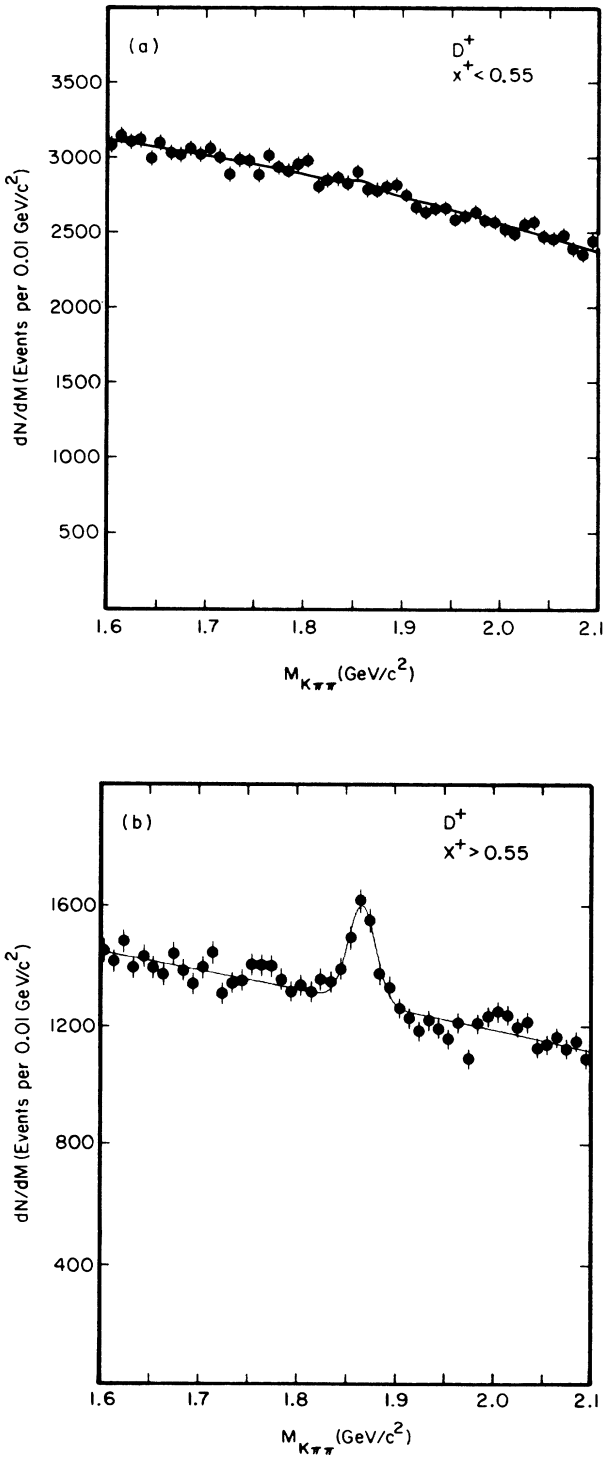

FIG. 2. The $K^-\pi^+\pi^+$ invariant-mass distribution for (a) $x^+ < 0.55$ and (b) $x^+ > 0.55$ showing the fit to the D^+ peak.

at low momenta, it is possible to estimate an upper limit for D^{*+} production, thereby calculating the rate of D^{*+} production required to account for all of the D^0's observed. Because of the very small Q value of the D^{*+} decay, the momentum, p_{D^0}, of a D^0 produced from the decay of a D^{*+} with momentum $p_{D^{*+}}$ can be approximated by

$$p_{D^0} \sim (m_{D^0}/m_{D^{*+}}) p_{D^{*+}} .$$

The region $0.0 < p_{D^0} < 1.5$ GeV/c is therefore fed by D^{*+}'s with $0.0 < p_{D^{*+}} < 1.7$ GeV/c with the uncertainty due to the nonzero Q value being around 5%. We have used this technique in Sec. IV B to obtain a measurement of D^{*+} production for $0.2 < x^+ < 0.43$.

D. D^{*0}

To identify a D^{*0}, we first designate as a D^0 candidate any $K^-\pi^+$ combination within ± 30 MeV of the known D^0 mass (1864.6 MeV) which cannot be identified as a $D^{*+} \to D^0\pi^+$ decay product when combined with other

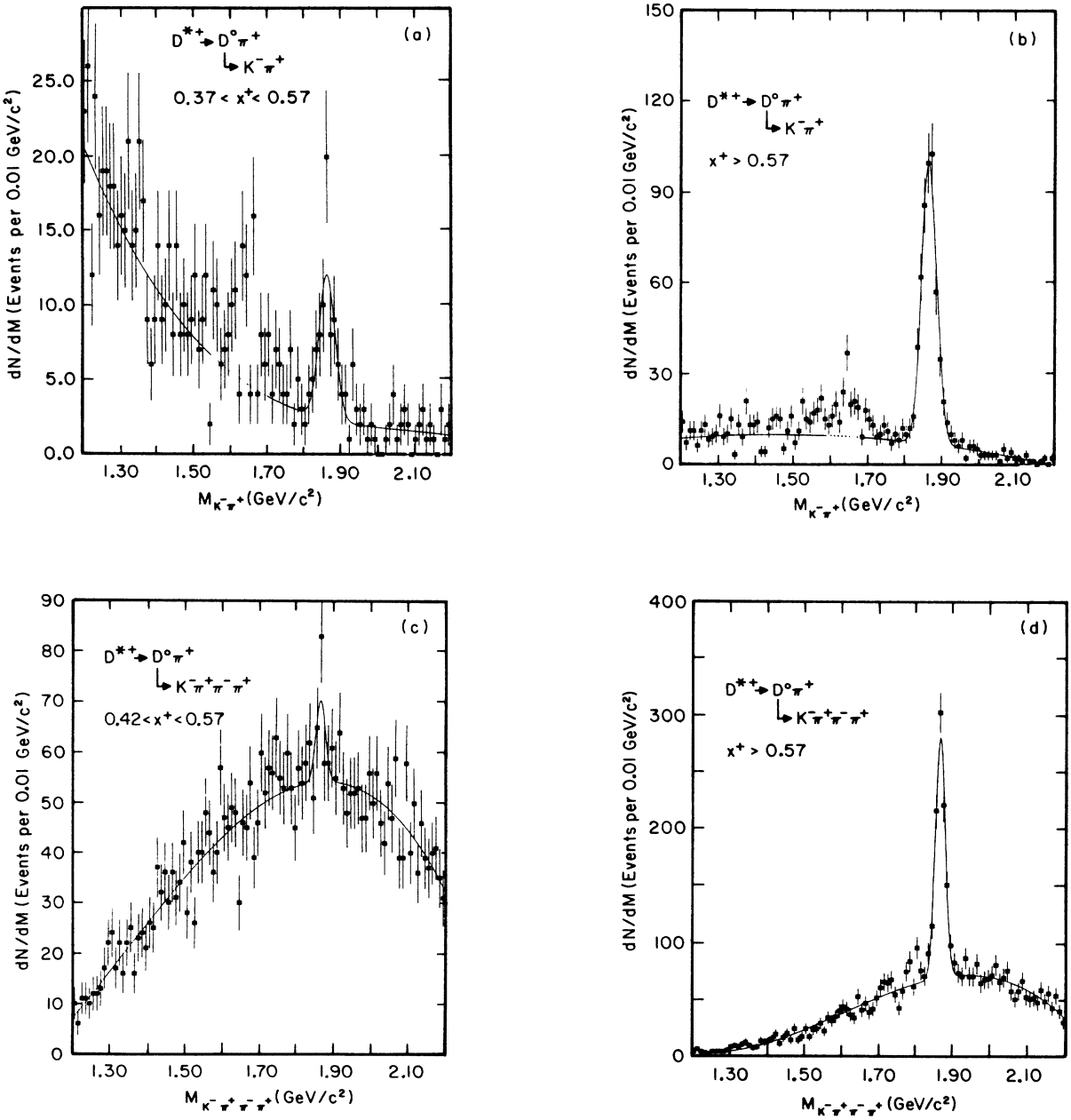

FIG. 3. The $K^-\pi^+$ invariant-mass distribution for $D^{*+} \to D^0\pi^+$, $D^0 \to K^-\pi^+$ candidates with (a) $0.37 < x^+ < 0.57$ and (b) $x^+ > 0.57$ and the similar $K^-\pi^+\pi^-\pi^+$ invariant-mass distribution for (c) $0.42 < x^+ < 0.57$ and (d) $x^+ > 0.57$. The fit to the D^0 peak is shown in each case.

charged tracks in the event. We combine the four-momentum of each D^0 candidate with that of each photon in the event which has not been identified as a π^0 daughter[29] and calculate the invariant mass $M(K\pi\gamma)$ of the combination. For the background determination we take $K\pi$ combinations from the upper D^0 sideband[30] ($1.91 < M_{K\pi} < 2.11$ GeV) and determine $M(K\pi\gamma)$ using their four-momenta. We then calculate the mass difference

$$\Delta M_D = [M(K\pi\gamma) - M(K\pi)]_{D \text{ region}}$$

and compare this with the quantity

$$\Delta M_{D,\text{ sideband}} = [M(K\pi\gamma) - M(K\pi)]_{\text{sideband region}} .$$

Evidence for the decay of the D^{*0} to the D^0 appears as a peak at low mass difference when we subtract the sideband from the signal mass distributions, normalized in the high mass-difference region. Because of our poor photon energy resolution, we are unable to resolve the peaks due to the direct decay $D^{*0} \to \gamma D^0$ and to the decay $D^{*0} \to D^0\pi^0$ ($\pi^0 \to \gamma\gamma$). In the latter case, we observe only one of the two π^0 daughter photons and obtain an apparent peak which is shifted down to approximately one-half of the $D^{*0} - D^0$ mass difference. We accordingly fit our observed signal to a sum of two Gaussians (Fig. 4) with the means and widths obtained from Monte Carlo simulation and the ratio of the two areas also obtained from Monte Carlo events when we input a $(D^{*0} \to D^0\gamma)/(D^{*0} \to D^0\pi^0)$ relative branching fraction of $(1 - 0.485)/0.485 = 1.06 \pm 0.32$ (Ref. 31).

Because of our relatively small photon-detection efficiency, for the D^{*0} analysis only we also used data samples taken previously at center-of-mass energies of 10.35 and 10.81–10.93 GeV, so that the total integrated luminosity for the D^{*0} analysis amounts to 290 pb^{-1}.

E. D_s

For the decay chain $D_s \to \phi\pi^+$, $\phi \to K^+K^-$, all K^+ and K^- candidates are required to satisfy kaon consistency in the dE/dx and time-of-flight measurements. A K^+K^- combination is required to have its invariant mass within 5 MeV of the known ϕ mass. Figure 5 shows the K^+K^- invariant-mass distribution with a peak at the ϕ mass. Any three-track $K^+K^-\pi^+$ combination for which the K^+K^- combination satisfies these ϕ criteria is considered a D_s candidate.

In order to improve the signal-to-noise ratio, additional requirements are made on decay angles. Since the D_s meson is spinless, the pion decay angle θ_π in the D_s center of mass must be isotropically distributed. The vector particle ϕ is aligned with respect to its direction of motion relative to the D_s, so that the distribution in θ_K, where θ_K is the decay angle, as previously defined, of the K^+ in the ϕ rest frame, is proportional to $\cos^2\theta_K$. In Fig. 6 we show the distributions of $\cos\theta_K$ and $\cos\theta_\pi$ for the D_s signal. There is good agreement between the measured and expected angular distributions. We require $\cos\theta_\pi > -0.8$, for which a 10% loss in signal is expected, and $|\cos\theta_K| > 0.4$, for which a 6.4% loss is predicted.

In Fig. 7 we show the resulting $\phi\pi$ mass spectrum for $x^+ > 0.56$.

F. Λ_c

In the case of the $\Lambda_c \to pK^-\pi^+$ decay, we require positive identification of the proton and consistency of the kaon. In order to reduce the background, the following cuts are applied: $p_p > 0.20$ GeV/c, $p_K > 0.15$ GeV/c, and $p_\pi > 0.30$ GeV/c. Proton identification and the cut on

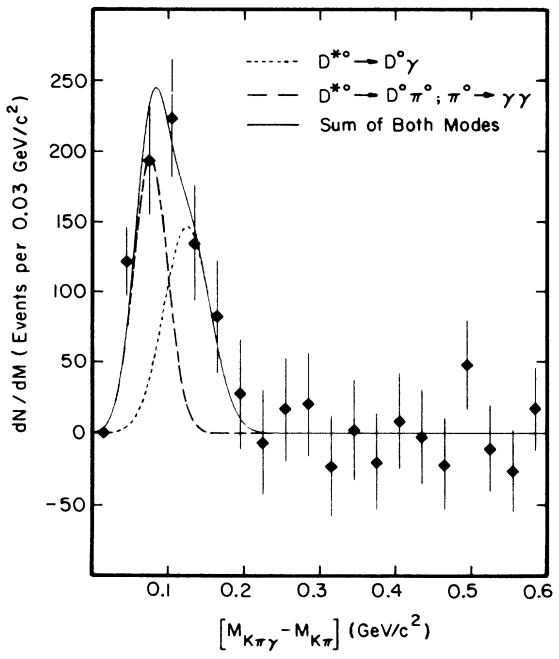

FIG. 4. The sideband-subtracted invariant-mass difference $m(K^-\pi^+\gamma) - m(K^-\pi^+)$ distribution for $x^+ > 0.51$. The curves are the fits to the expected shapes for the decays $D^{*0} \to D^0\pi^0$ and $D^{*0} \to D^0\gamma$ and their sum.

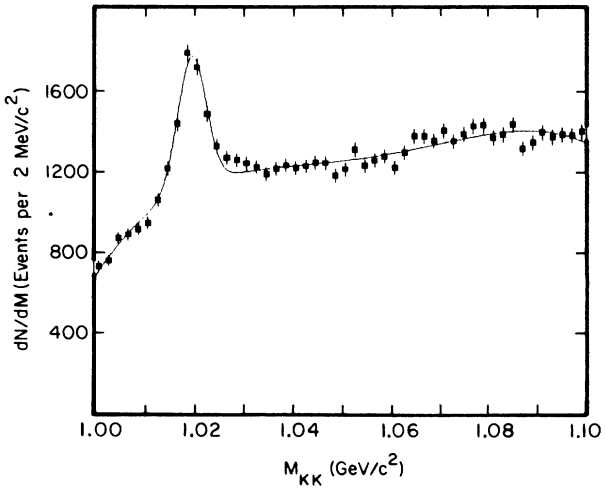

FIG. 5. The K^+K^- invariant-mass distribution showing the fit to the ϕ peak.

the pion momentum are the most effect in reducing the background.

The efficiency for positive proton identification varies from 95% at the lowest momenta to 10% at 2.0 GeV/c. A systematic error of 18% on the production cross section has been estimated by changing the particle identification criteria and the momentum cuts.

The $pK^-\pi^+$ invariant-mass distribution for $x > 0.50$ is shown in Fig. 8.

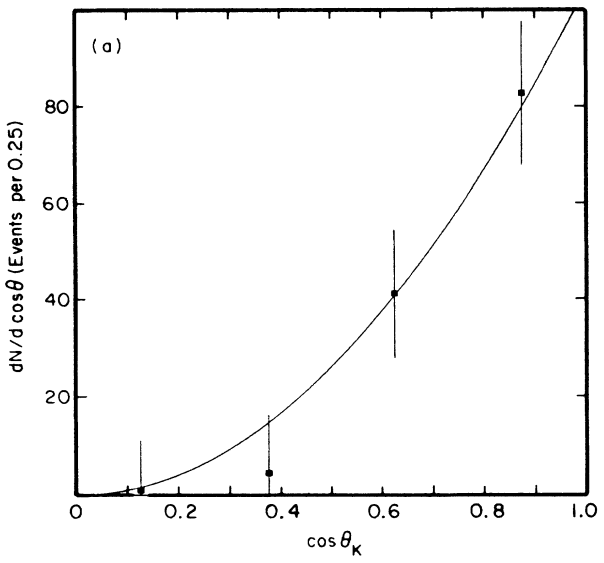

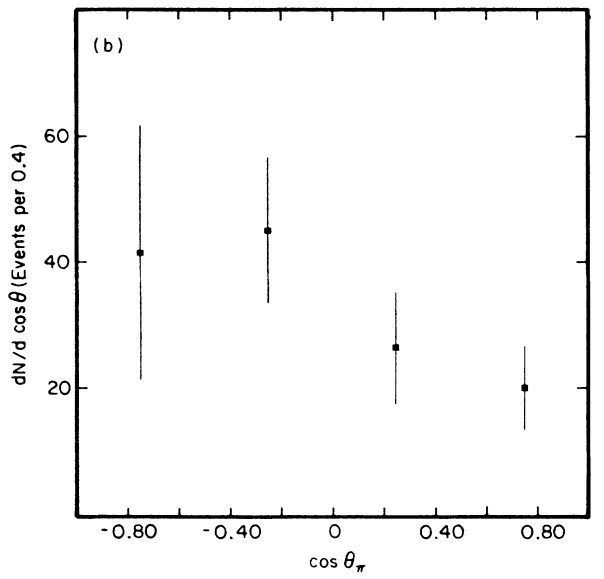

FIG. 6. (a) The $\cos\theta_K$ distribution for the decay chain $D_s \to \phi\pi^+$, $\phi \to K^+K^-$, where θ_K is the decay angle of the K^+ in the ϕ rest frame. The curve is the expected $\cos^2\theta_K$ behavior. (b) The $\cos\theta_\pi$ distribution for the decay $D_s \to \phi\pi^+$, where θ_π is the decay angle of the π^+ in the D_s rest frame.

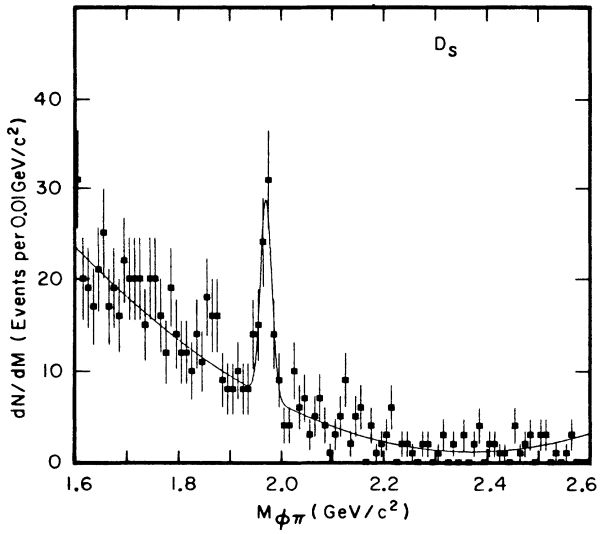

FIG. 7. The $\phi\pi^+$ invariant-mass distribution for $x^+ > 0.56$ showing the fit to the D_s peak.

IV. DIFFERENTIAL AND TOTAL CROSS SECTIONS

In this section we present our results on the differential and total cross sections for the production of charmed hadrons and their comparison with the results of other experiments. We start by introducing the variables with respect to which we have measured the differential cross sections.

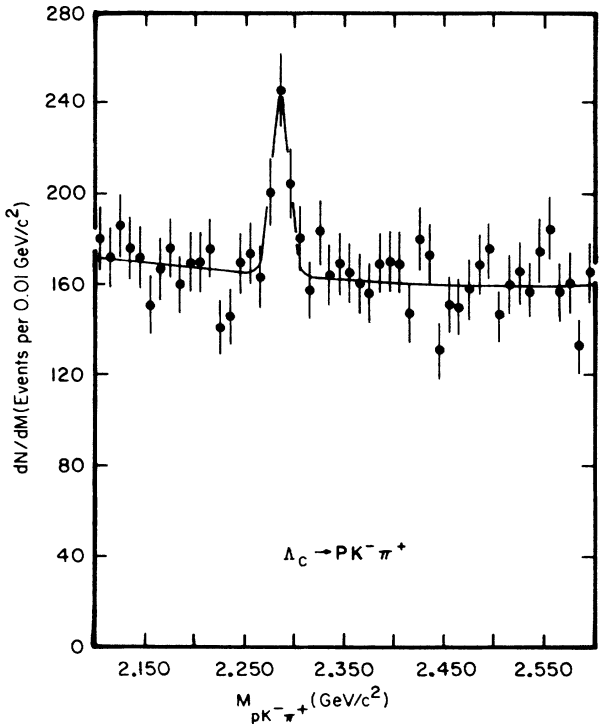

FIG. 8. The $pK^-\pi^+$ invariant-mass distribution showing the fit to the Λ_c peak for all values of x^+.

A. Choice of fragmentation variables

Two commonly used scaling variables are

$$x = p/p_{\max} \quad \text{and} \quad x^+ = \frac{E+p_\parallel}{E_{\max}+p_{\max}} , \tag{8}$$

where p and E are the momentum and energy of the hadron and $p_\parallel$ is the component of p along the jet axis; $E_{\max}$ and $p_{\max}$ are the corresponding maximum attainable values.

We define $p_{\max}$ as

$$p_{\max} = (E_{\text{beam}}^2 - m^2)^{1/2} , \tag{9}$$

where m is the mass of the hadron in question. The D^* can be produced with a $\bar{D}$ rather than a $\bar{D}^*$, giving a slightly higher value of $p_{\max}$ than given by (9); however, the difference of 0.5% is negligible.

Within any parton fragmentation model the definitions of the variables x and x^+ would have as the denominator the (unknown) respective quantities for the primary charm quark rather than the kinematical limit for the charmed hadron under consideration. The two choices differ because of the mass of the quark and especially because of gluon bremsstrahlung. We shall discuss the QCD radiative corrections later.

The variable most widely used in the context of the string fragmentation model is the light-cone variable x^+. It has the advantage of being a relativistic invariant for boosts in the direction of the primary quark motion. Not knowing the direction of the initial quark and not being able to estimate reliably even the jet direction, we substitute the magnitude of the hadron momentum for its longitudinal component:

$$x^+ = \frac{E+p}{(E+p)_{\max}} . \tag{10}$$

We have used the Lund Monte Carlo procedure[32] to study the effect of this substitution. Figure 9 shows the D^* distribution in x^+, defined in Eq. (10) divided by the corresponding variable using Eq. (8). The distortion of the distribution is minimal except for $x^+ < 0.35$, where our D^{*+} acceptance vanishes.

B. Experimental fragmentation distributions

The experimental fragmentation distributions $B\,d\sigma/dx^+$, uncorrected for decay branching fractions B (except in the case of $\phi \to K^+K^-$), for D^{*+}, D^0, D^+, D_s, and Λ_c are shown in Figs. 10–14. The curves shown in the figures will be described in Sec. VII B. In Tables I–V we give, bin by bin, the reconstruction efficiency, the raw yield of events, the differential cross section $B\,d\sigma/dx^+$, and the fully corrected, scaling cross section $s\,d\sigma/dx^+$. (The decay branching fractions used for the latter are listed in Table IX.) Our measurements have been appropriately scaled to represent the cross section at $\sqrt{s} = 10.55$ GeV. The errors shown in Tables I–V and in Figs. 10–15 are due to the statistical accuracy of the data sample and to uncertainties in the simulations used to obtain the detection efficiencies. Negative values of the differential cross sections, whenever they result from background fluctuations in the fitting procedure, are listed in order to arrive at the correct upper limit to the differential cross section in that bin. In Table I the results for the two observed decay modes of D^{*+} are separately shown. When scaled for the different D^0 decay branching fractions, these two distributions are con-

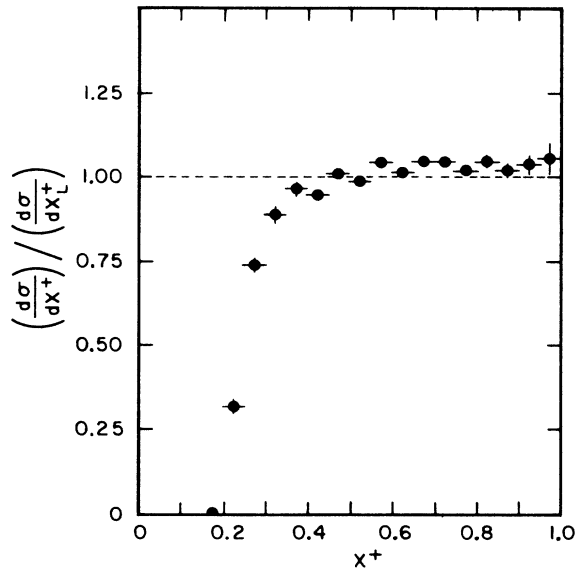

FIG. 9. The ratio of the Lund Monte Carlo D^* fragmentation distribution using the variable x^+ as defined in Eq. (8) to that using the correct light-cone variable.

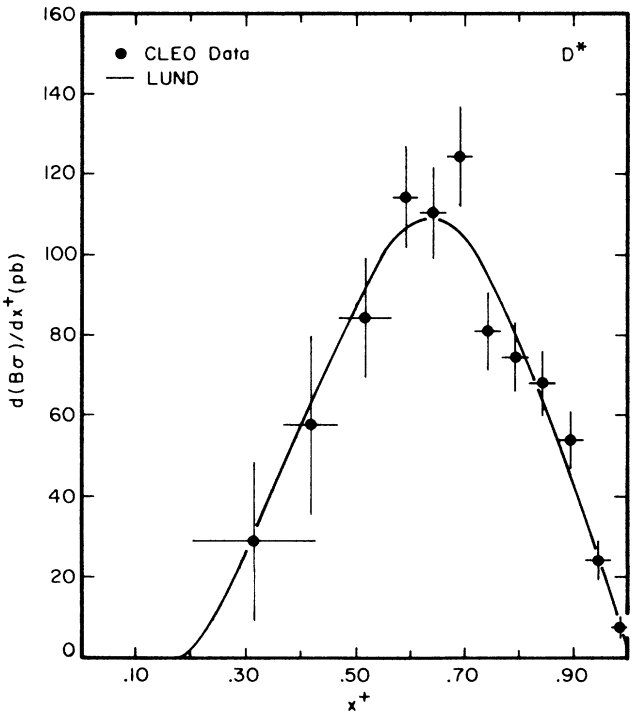

FIG. 10. The experimental D^{*+} fragmentation distribution $B\,d\sigma/dx^+$. The curve is a fit to the distribution predicted by the Lund Monte Carlo procedure.

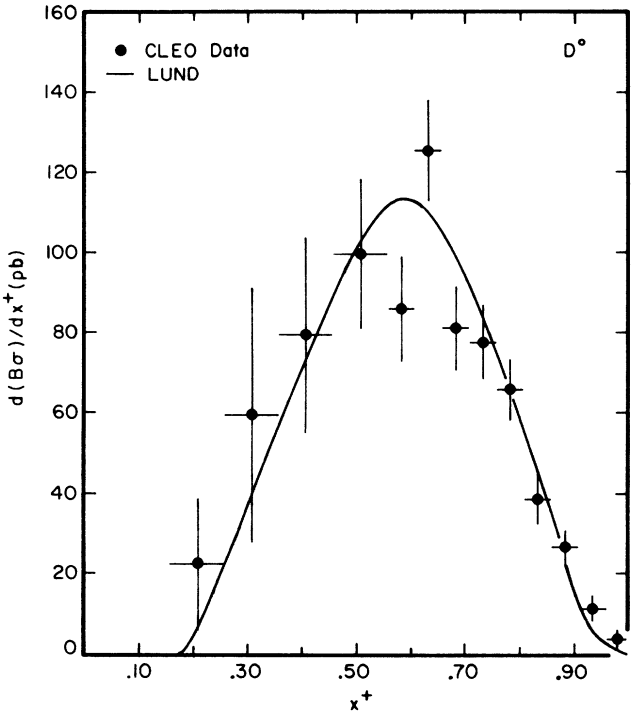

FIG. 11. The experimental D^0 fragmentation distribution $B\,d\sigma/dx^+$. The curve is a fit to the distribution predicted by the Lund Monte Carlo procedure.

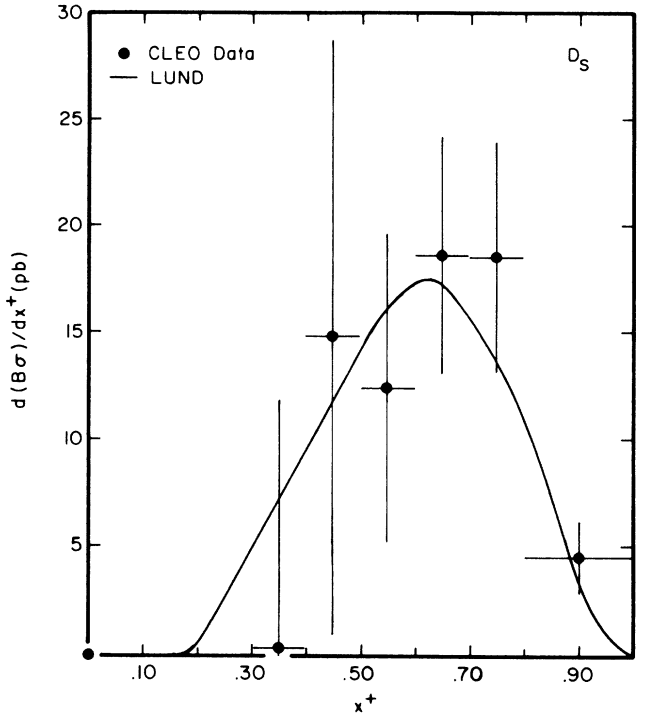

FIG. 13. The experimental D_s fragmentation distribution $B\,d\sigma/dx^+$. The curve is a fit to the distribution predicted by the Lund Monte Carlo procedure.

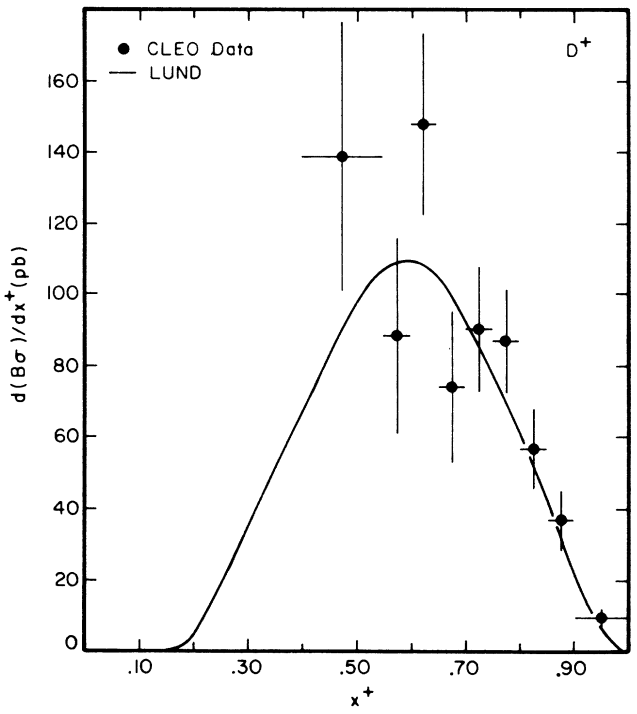

FIG. 12. The experimental D^+ fragmentation distribution $B\,d\sigma/dx^+$. The curve is a fit to the distribution predicted by the Lund Monte Carlo procedure.

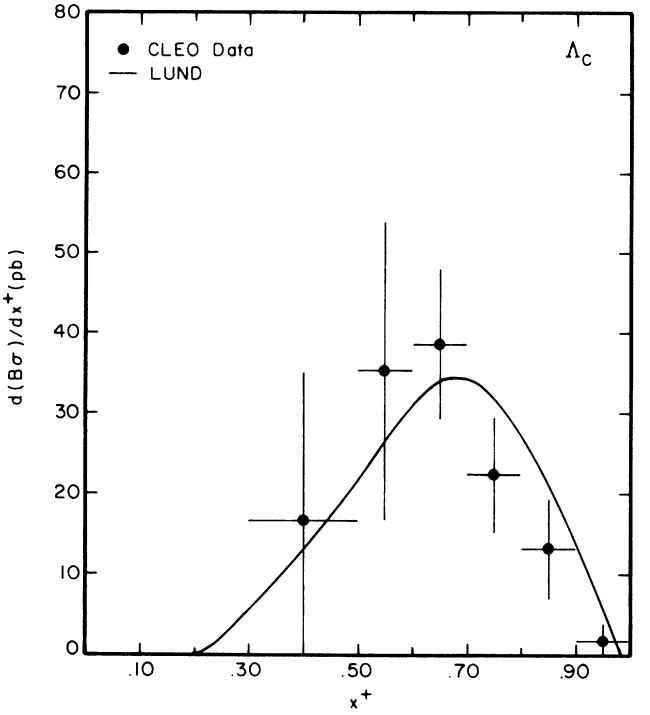

FIG. 14. The experimental Λ_c fragmentation distribution $B\,d\sigma/dx^+$. The curve is a fit to the distribution predicted by the Lund Monte Carlo procedure.

TABLE I. D^{*+} fragmentation data, x^+ variable.

x^+	Efficiency	Yield	$B\frac{d\sigma}{dx^+}$ (pb)	$s\frac{d\sigma}{dx^+}$ (GeV^{2}nb)
	(a) $D^{*+}\to D^0\pi^+$, $D^0\to K^-\pi^+$			
0.37–0.47	0.19±0.01	13±5	19±7	82±32
0.47–0.57	0.31±0.01	29±6	27±6	119±25
0.57–0.62	0.35±0.02	80±10	40±5	177±24
0.62–0.67	0.37±0.02	80±10	38±5	168±23
0.67–0.72	0.38±0.02	96±11	44±6	195±25
0.72–0.77	0.39±0.03	52±9	23±4	104±19
0.77–0.82	0.40±0.03	47±8	21±4	93±17
0.82–0.87	0.40±0.03	45±8	20±4	88±17
0.87–0.92	0.41±0.03	36±7	16±3	69±15
0.92–0.97	0.42±0.03	13±5	6±2	24±10
0.97–1.00	0.43±0.03	3±2	2±1	9±5
	(b) $D^{*+}\to D^0\pi^+$, $D^0\to K^-\pi^+\pi^+\pi^-$			
0.47–0.57	0.18±0.02	38±12	59±20	120±41
0.57–0.62	0.23±0.02	88±15	68±13	139±27
0.62–0.67	0.25±0.02	100±13	70±11	143±23
0.67–0.72	0.27±0.02	117±16	76±12	154±25
0.72–0.77	0.29±0.02	101±14	62±10	126±21
0.77–0.82	0.30±0.03	98±12	58±9	119±17
0.82–0.87	0.31±0.03	87±11	50±8	102±16
0.87–0.92	0.31±0.03	70±10	40±7	82±14
0.92–0.97	0.31±0.03	39±8	22±5	46±10
0.97–1.00	0.30±0.03	8±4	8±4	16±8

TABLE II. D^0 fragmentation data, x^+ variable.

x^+	Efficiency	Yield	$B\frac{d\sigma}{dx^+}$ (pb)	$s\frac{d\sigma}{dx^+}$ (GeV^{2}nb)
0.16–0.26	0.61±0.02	50±37	22±17	59±44
0.26–0.36	0.57±0.02	123±65	59±32	157±84
0.36–0.46	0.54±0.02	156±48	79±24	209±64
0.46–0.56	0.53±0.02	191±36	100±19	262±49
0.56–0.61	0.53±0.02	257±40	86±13	229±35
0.61–0.66	0.53±0.02	378±38	125±13	334±34
0.66–0.71	0.54±0.02	248±32	81±11	216±28
0.71–0.76	0.54±0.02	237±28	77±9	206±25
0.76–0.81	0.55±0.02	205±25	66±8	175±21
0.81–0.86	0.56±0.02	123±20	39±6	103±17
0.86–0.91	0.57±0.02	86±15	27±5	71±12
0.91–0.96	0.58±0.02	38±11	11±3	30±8
0.96–1.00	0.59±0.02	13±8	4±2	11±6

TABLE III. D^+ fragmentation data, x^+ variable.

x^+	Efficiency	Yield	$B\frac{d\sigma}{dx^+}$ (pb)	$s\frac{d\sigma}{dx^+}$ (GeV^{2}nb)
0.20–0.40	0.38±0.01	−34±26	−51±39	−62±47
0.40–0.55	0.37±0.01	92±25	139±38	166±46
0.55–0.60	0.37±0.01	186±58	88±28	106±33
0.60–0.65	0.37±0.01	314±55	148±26	177±31
0.65–0.70	0.38±0.01	159±46	74±21	89±26
0.70–0.75	0.38±0.01	197±38	90±18	108±21
0.75–0.80	0.39±0.01	193±32	87±15	104±17
0.80–0.85	0.40±0.01	128±25	57±11	68±14
0.85–0.90	0.41±0.01	85±19	37±8	44±10
0.90–1.00	0.42±0.01	22±6	9±3	11±3

sistent with each other, the relative χ^2 being 8.2 for nine degrees of freedom. The two results have been combined in Fig. 10 and also in Fig. 15 (Ref. 33), where we show the fully corrected, scaling fragmentation distribution $s\,d\sigma/dx^+$ for D^* compared with data from the ARGUS Collaboration.[20] The ARGUS data were scaled by 0.610 to take into account the different decay branching fractions used. The agreement is excellent. The curve in Fig. 15 will be discussed later.

Because of the large statistical errors due to the small signal-to-background ratio, the D^{*0} sample was divided into only two x^+ intervals. In Table VI we give the information as in the previous tables for the two x^+ intervals, including the systematic uncertainty in the modeling of the detection efficiency.

In the case of the D_s and Λ_c, no fully corrected differential cross sections are listed because of the large uncertainty in their decay branching fractions.

C. Comparison with PEP and PETRA results

As has been noted by Bethke[34] and others, the comparison of data at CESR energies to that of PEP and/or PETRA requires an understanding of how the large QCD radiative corrections change with increasing center-of-mass energy.

For this study we use only the D^{*+} sample because similar measurements exist at the PEP/PETRA energies.[12–14,16,19] Furthermore, this sample is statistically the most accurate, has the least background, and is measured through two different D^0 decay modes, allowing a check of the systematic errors. For the fragmentation variable we use x^+ since that, being Lorentz invariant, facilitates the comparison of data at various energies.

Our method of comparison uses an evolution equation for QCD which relates the fragmentation function at one center-of-mass energy to that at another energy, incorporating the radiation of gluons.[35] Such an evolution softens the x^+ spectrum of the D^{*+} as the center-of-mass energy is increased, since more of the available energy goes into gluons which themselves fragment into other hadrons. The form of the equation we use is[35]

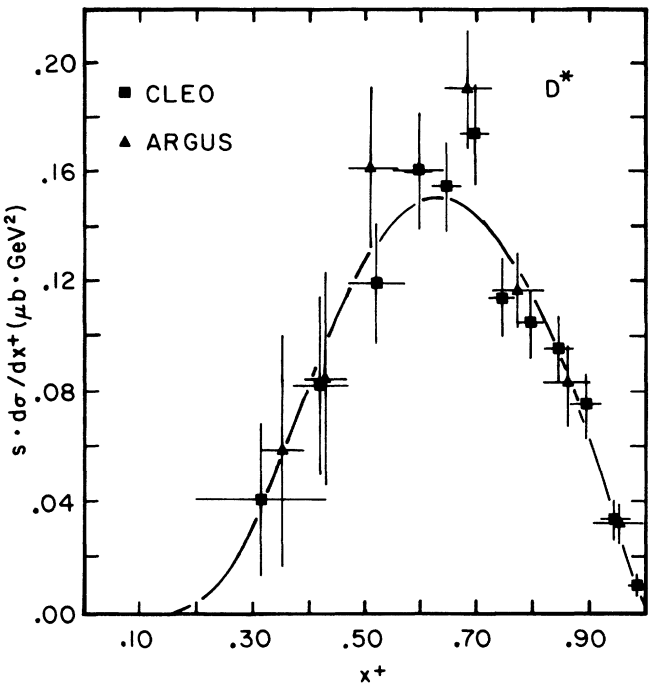

FIG. 15. The fully corrected, scaling D^{*+} fragmentation distribution $s\,d\sigma/dx^+$ from the CLEO experiment (squares) and from the ARGUS experiment (triangles). The curve is a direct fit to the CLEO distribution using the analytical, theoretical fragmentation function of Andersson *et al.* (Table X).

$$\frac{dD(x^+,t_0)}{dt}=\frac{24}{75t_0}\left[\int_{x^+}^{1}\frac{1+z^2}{1-z}\left[\frac{D(x^+/z,t_0)}{z}-D(x^+,t_0)\right]dz+D(x^+,t_0)\left[x^++\frac{(x^+)^2}{2}+2\ln(1-x^+)\right]\right],$$

where $D(x^+,t)$ is the fragmentation function at a particular dimensionless energy defined as $t=\ln(s/\Lambda^2)$, where Λ is the QCD parameter. We then use our D^{*+} distribution from Fig. 10 as $D(x^+,t_0)$ at $\sqrt{s}=10.55$ GeV and evolve the distribution to $\sqrt{s}=30.4$ GeV, which is an average of the PEP and PETRA center-of-mass energies. The analysis assumes four quark flavors (to calculate the two numerical parameters 24 and 75), a QCD parameter

TABLE IV. D_s fragmentation data, x^+ variable.

x^+	Efficiency	Yield	$B\frac{d\sigma}{dx^+}$ (pb)
0.20–0.30	0.08±0.01	2.1±1.5	−8±5
0.30–0.40	0.09±0.01	0.1±3.7	0±12
0.40–0.50	0.08±0.01	4.3±4.0	15±14
0.50–0.60	0.08±0.01	11.5±6.7	12±7
0.60–0.70	0.10±0.01	20.6±6.2	19±6
0.70–0.80	0.09±0.01	19.7±5.8	19±5
0.80–1.00	0.11±0.01	11.3±4.3	5±2

TABLE V. Λ_c fragmentation data, x^+ variable.

x^+	Efficiency	Yield	$B\frac{d\sigma}{dx^+}$ (pb)
0.22–0.30	0.30±0.04	−13±15	−15±17
0.30–0.50	0.24±0.02	29±32	17±18
0.50–0.60	0.23±0.02	30±15	35±19
0.60–0.70	0.21±0.02	93±21	39±9
0.70–0.80	0.19±0.02	49±15	22±7
0.80–0.90	0.14±0.02	21±9	13±6
0.90–1.00	0.20±0.03	4±5	2±2

TABLE VI. D^{*0} fragmentation data, x^+ variable. $D^{*0}\to D^0\gamma$ or $D^0\pi^0$, $D^0\to K^-\pi^+$.

x^+	Efficiency	Yield	$B\frac{d\sigma}{dx^+}$ (pb)	$s\frac{d\sigma}{dx^+}$ (GeV^{2}nb)
0.51–0.66	0.13±0.03	413±59	72±10±17	190±27±44
0.66–1.00	0.14±0.03	345±42	25±3±6	65±8±15

TABLE VII. PEP and PETRA D^{*+} data.

TASSO (Ref. 16)

Obtained from plot		Calculated for x^+	
Range in z	$(s/\beta)d\sigma/dz$ (μb/GeV^2)	Range in x^+	$s\,d\sigma/dx^+$ (μb/GeV^2)
0.30–0.40	0.03±0.17	0.289–0.393	0.027±0.155
0.40–0.50	0.08±0.11	0.393–0.495	0.076±0.104
0.50–0.60	0.33±0.12	0.495–0.596	0.318±0.115
0.60–0.70	0.27±0.09	0.596–0.697	0.262±0.087
0.70–0.80	0.26±0.09	0.697–0.798	0.254±0.088
0.80–0.90	0.10±0.06	0.798–0.899	0.098±0.059
0.90–1.00	0.01±0.04	0.899–1.000	0.010±0.039

JADE (Ref. 19)

Obtained from plot		Calculated for x^+	
Range in z	$s\,d\sigma/dz$ (μb/GeV^2)	Range in x^+	$s\,d\sigma/dx^+$ (μb/GeV^2)
0.28–0.40	0.04±0.13	0.268–0.391	0.039±0.125
0.40–0.52	0.29±0.09	0.391–0.515	0.284±0.088
0.52–0.64	0.54±0.12	0.515–0.637	0.532±0.118
0.64–0.76	0.30±0.11	0.637–0.758	0.297±0.109
0.76–0.88	0.15±0.09	0.758–0.879	0.149±0.089
0.88–1.00	0.11±0.09	0.879–1.000	0.109±0.089

HRS (Ref. 13)

Obtained from table		Calculated for x^+	
Range in z	$(s/\beta)d\sigma/dz$ (μb/GeV^2)	Range in x^+	$s\,d\sigma/dx^+$ (μb/GeV^2)
0.20–0.40	0.168±0.049	0.173–0.389	0.134±0.039
0.40–0.50	0.185±0.060	0.389–0.493	0.171±0.055
0.50–0.60	0.391±0.070	0.493–0.595	0.370±0.066
0.60–0.70	0.211±0.050	0.595–0.696	0.203±0.048
0.70–0.80	0.118±0.035	0.696–0.798	0.114±0.034
0.80–1.00	0.026±0.011	0.798–1.000	0.025±0.011

TPC (Ref. 14)

Obtained from table		Calculated for x^+	
Range in z	$(s/\beta)d\sigma/dz$ (μb/GeV^2)	Range in x^+	$s\,d\sigma/dx^+$ (μb/GeV^2)
0.20–0.30	0.00±0.10	0.173–0.284	0.000±0.074
0.30–0.40	0.21±0.07	0.284–0.389	0.183±0.061
0.40–0.50	0.22±0.07	0.389–0.493	0.203±0.065
0.50–0.60	0.25±0.07	0.493–0.595	0.237±0.066
0.60–0.70	0.33±0.08	0.595–0.696	0.317±0.077
0.70–0.80	0.15±0.06	0.696–0.798	0.145±0.058
0.80–0.90	0.08±0.04	0.798–0.899	0.078±0.039
0.90–1.00	0.04±0.02	0.899–1.000	0.039±0.195

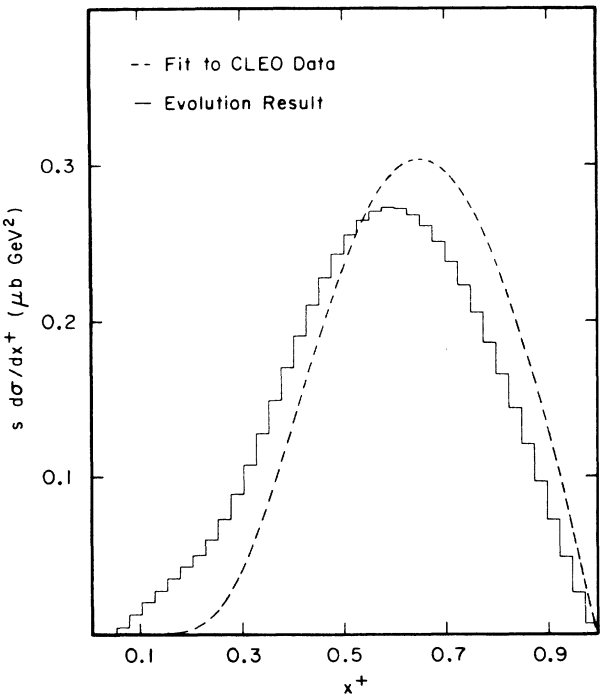

FIG. 16. A fit to the CLEO D^{*+} fragmentation distribution (dashed curve) and the evolution of this distribution to a center-of-mass energy of 30.4 GeV (solid curve).

of $\Lambda = 0.200$ GeV, and an energy step size of $\Delta\sqrt{s} = 0.50$ GeV; variations in these parameters produce differences insignificant on the scale of the present experimental uncertainties. After each iteration, $D(x^+,t)$ is set to zero for unphysical regions of x^+. The result of the evolution procedure is indicated in Fig. 16, where the dashed curve is a fit to our data and the solid line the result after evolution.

Listed in Table VII are the D^{*+} fragmentation distributions of the TASSO (Ref. 16) and JADE (Ref. 19) Collaborations at PETRA and of the HRS (Ref. 13) and TPC (Ref. 14) experiments at PEP. Both the published results (in the variable $z \equiv E/E_{\max}$) and the results of converting to $(s\,d\sigma/dx^+)$ vs x^+ are given. No attempt has been made to subtract the contamination from B decay or to alter the distributions for QED radiation. We then take the form from the fitted CLEO D^{*+} data and that from the evolution prescription and vary only the normalizations in attempting to fit the PEP/PETRA results. To eliminate D^{*+}'s produced via B meson decay, we have only used data for $x^+ > 0.4$ in the fitting procedure.

TABLE VIII. Fits to PEP/PETRA data.

Experiment	CLEO shape χ^2/DF	Evolution shape χ^2/DF
TASSO (PETRA)	3.5/5	2.8/5
JADE (PETRA)	4.9/4	2.9/4
HRS (PEP)	29.0/4	18.0/4
TPC (PEP)	6.8/6	2.9/6

The χ^2 from fitting each experiment's data to our data and to the evolved distribution are listed in Table VIII and depicted in Figs. 17(a)–17(d). With the exception of the HRS data, the agreement is very good and demonstrates the usefulness of this evolution procedure in comparing spectra obtained at different center-of-mass energies. Even in the comparison with the HRS data, the distribution evolved to $\sqrt{s} = 30.4$ GeV gives a much better χ^2 than the original data at $\sqrt{s} = 10.55$ GeV.

D. The total cross sections

In the low-momentum region, $x < 0.50$ ($x^+ < 0.55$), the statistical accuracy of our data is poor since the combinatorial background is large and we are restricted to the continuum sample in order to avoid including charmed particles from B decay. Furthermore, the D^{*+} acceptance drops to zero for $x < 0.3$ ($x^+ < 0.4$). We therefore present in Table IX our measured products of cross section times decay branching fraction, $B\sigma$, integrated over the interval $0.50 < x < 1.0$ ($0.55 < x^+ < 1.0$).

To find the total cross sections, we extrapolate over the unseen part of the momentum spectrum. In the case of the D^{*+} we use our fits to the theoretical fragmentation models described later in Sec. VII C. The spread of values for the integrals of the fitted fragmentation functions is less than the statistical error. We quote as a total $B\sigma$ the mean of these values and assign their rms spread as a systematic error.

For the D^0, D^+, D_s, and Λ_c the models used to describe the fragmentation distributions are not expected to be meaningful because of the large feed down from heavier charmed particles. However, we have used those models which adequately fit the data in order to extrapolate to low momenta, as was done for the D^{*+}. Again, we use the spread in the resulting values as a measure of the systematic error. The measured $B\sigma$ ($x > 0.50$), the extrapolated $B\sigma$, and the total cross sections, with the decay branching fractions used, are given in Table IX. In order to obtain the total cross section for D^{*0} production, we assume that the shape of the differential cross section is the same as that of the D^{*+}. The total cross section so obtained is consistent with that for D^{*+} production. It is one of the best measurements of D^{*0} production cross section in e^+e^- annihilation.

E. The total cross section into charmed particles

Using the extrapolated cross sections for D^0 and D^+ and the branching fractions measured by the Mark III Collaboration,[36] we calculate the total inclusive cross section for D^0 and D^+ production. The result is $\sigma(D^0+D^+) = 1.76 \pm 0.15 \pm 0.18$ nb, where the first error is our statistical and systematic uncertainties added in quadrature, while the second error is from the quoted[36] uncertainties in the D decay branching fractions. The total hadronic continuum cross section at $\sqrt{s} = 10.55$ GeV is $3.33 \pm 0.05 \pm 0.21$ nb (Ref. 37). Based on a Monte Carlo study that takes into account initial-state bremsstrahlung and our event-selection efficiency, we find that $c\bar{c}$ should account for $(37 \pm 2)\%$ of the total annihilation cross section into hadrons, where the error is largely due to the

uncertainty in the choice for the maximum photon energy allowed in the initial-state QED radiative corrections. Thus, we expect a charm contribution of $2\times0.37\times3.33$ nb$=2.46\pm0.04\pm0.20$ nb. With that assumption, our measured D^0+D^+ production accounts for $(71\pm6\pm10)\%$ of the expected total charmed-hadron production cross section.[38] The HRS group[39] finds a similar value of $(60\pm10)\%$ for the (D^0+D^+) fraction of the expected charm cross section for e^+e^- annihilation at $\sqrt{s}=29$ GeV. Our results imply that as much as $(29\pm6\pm10)\%$ of the charm cross section goes into D_s and charmed baryons. The lack of accurate measurements of the D_s

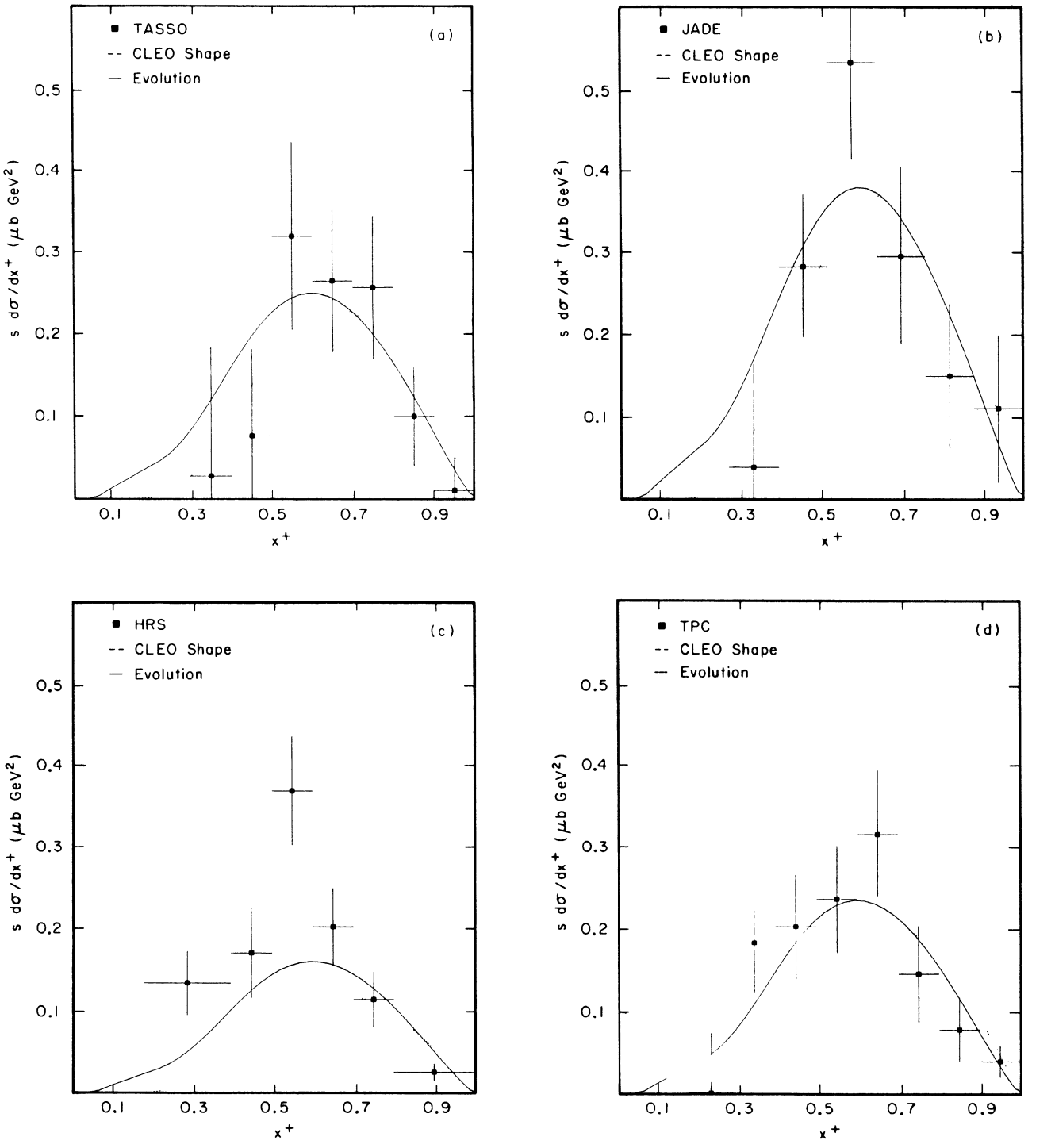

FIG. 17. Comparison of the evolved CLEO D^{*+} fragmentation distribution from Fig. 16 (solid curve) and a fit to the CLEO data (dashed curve) with the experimental distribution from (a) the TASSO experiment, (b) the JADE experiment, (c) the HRS experiment, and (d) the TPC experiment.

TABLE IX. Total cross sections, $\sqrt{s} = 10.55$ GeV.

Decay	Sample size	$B\sigma(x>0.50)$[a] (pb)	$B\sigma$[b] (pb)	σ_{tot}[c] (nb)
$D^0 \to K^-\pi^+$	2244±123	27.0±1.4	52±5±4	1.24±0.11±0.05±0.17
$D^+ \to K^-\pi^+\pi^+$	1376±112	29.3±2.5	47±7±2	0.52±0.08±0.02±0.08
$D^{*+} \to D^0\pi^+$				0.77±0.05±0.05±0.12[d]
$\quad \hookrightarrow K^-\pi^+$	494±26	10.9±0.6	17.0±1.5±1.4	
$\quad \hookrightarrow K^-\pi^+\pi^-\pi^+$	746±38	23.1±1.2	33.0±3.0±1.8	
$D^{*0} \to D^0(\gamma \text{ or } \pi^0)$				
$\quad \hookrightarrow K^-\pi^+$	758±73	19.8±1.9±3.3[e]	30.0±3.0±5.8[f]	0.74±0.07±0.14±0.10
$D_s \to \phi\pi^+$				
$\quad \hookrightarrow K^+K^-$	70±13	5.8±1.0	7.2±1.9±1	g
$\Lambda_c \to pK^-\pi^+$	226±45	8.6±1.4	13.5±4.0±1.4	g

[a]Cross section times branching ratio, $B\sigma$ for $x > 0.50$, for the production of the charmed hadrons detected through the listed decay modes.

[b]Extrapolated $B\sigma$: values from a, scaled by a factor determined from extrapolation of the fitted functions. The first error is the statistical one from fitting the functions; the second is obtained from the variation of the scaling factors for different functions. See f below for the special case of the D^{*0}.

[c]The branching fractions used are $B(D^0 \to K^-\pi^+) = (4.2\pm0.4\pm0.4)\%$ (Ref. 36), $B(D^0 \to K^-\pi^+\pi^-\pi^+) = (9.1\pm0.8\pm0.8)\%$ (Ref. 36), $B(D^+ \to K^-\pi^+\pi^+) = (9.1\pm1.3\pm0.4)\%$ (Ref. 36), $B(D^{*+} \to D^0\pi^+) = (52\pm7\pm11)\%$, derived in Sec. V, $B(\phi \to K^+K^-) = (49\pm1)\%$ (Ref. 31). The third error for σ_{tot} is due to the uncertainties in these branching fractions.

[d]Weighted average of results for the two decay modes.

[e]The second error is due to the uncertainty in the relative branching ratio of the two decay modes.

[f]Assuming that the shape of the differential cross section is the same as that of the D^{*+}, we used the scaling factor used for the D^{*+}. The first, statistical error is just scaled from the previous column; the second, systematic error combines the scaled, systematic error from the previous column with the error in the scaling factor.

[g]The lack of knowledge of the decay branching fraction does not allow us to calculate the corrected cross section.

and Λ_c decay branching fractions makes it impossible to check this conclusion.

F. Relative decay branching ratio for D^0

Since we have measured the D^{*+} cross section independently for two D^0 decay modes, the ratio of the two cross sections gives the relative branching fraction of the two modes. For the interval $0.50 < x < 1.0$ where we have the best accuracy, we get

$$\sigma B(D^{*+} \to (K^-\pi^+)\pi^+) = 10.9\pm0.6\pm0.4 \text{ pb} ,$$

$$\sigma B(D^{*+} \to (K^-\pi^+\pi^-\pi^+)\pi^+) = 23.1\pm1.2\pm0.9 \text{ pb} ,$$

where the second error is the systematic error discussed in Sec. IV D. We thus get the ratio

$$\frac{B(D^0 \to K^-\pi^+\pi^-\pi^+)}{B(D^0 \to K^-\pi^+)} = 2.12\pm0.16\pm0.09 .$$

This result may be compared to the values reported by the Mark III Collaboration,[36] 2.17±0.28±0.28, and by the ARGUS group,[20] 2.17±0.28±0.23.

V. VECTOR TO PSEUDOSCALAR RATIO AND THE D^{*+} DECAY BRANCHING RATIO

From our measurement of D^{*0}, D^{*+}, D^0, and D^+ production cross sections we can extract two quantities of interest: the D^{*+} decay branching fraction $B_* \equiv B(D^{*+} \to D^0\pi^+)$ and the probability P_V for a charmed meson to be produced with spin 1. The four available cross-section values provide redundant information and can be used in different ways to calculate B_*, P_V, and their product. The equations used to calculate these quantities and the weighted averaging procedure to combine the different results in the best estimate of B_* and P_V are described in Appendix A. The important assumptions are that the D^{*0} and D^{*+} production cross sections are equal and the cross sections for the direct production of D^0 and D^+ are also equal.

For the branching fraction $B_* \equiv B(D^{*+} \to D^0 + \pi^+)$ we obtain

$$B_* = 0.52\pm0.07\pm0.11 . \quad (11)$$

This value should be compared with the previous results of Goldhaber *et al.*[41] (0.60±0.15), of Coles *et al.*[42] (0.44±0.07), and with the recent preliminary result (0.55±0.02±0.06) of the Mark III Collaboration.[43]

For the probability P_V for a charmed meson to be produced as a vector meson we obtain the result

$$P_V = 0.85\pm0.11\pm0.17 . \quad (12)$$

Based on spin counting, one naively expects $P_V = 0.75$. Buchanan and Chun[44] have modified the Lund fragmentation model doing away with strangeness and diquark suppression parameters, relying completely on the hadron masses to differentiate the production of baryons and strange particles from that of ordinary mesons. For charmed mesons they predict $P_V = 0.63$, which is lower than, but not incompatible with our result.

As shown in Appendix A, the product $B_* P_V$ can be

calculated directly from the measured D^* and D-production cross sections giving the result

$$B_* P_V = 0.44 \pm 0.04 \pm 0.05 \ . \tag{13}$$

VI. FRAGMENTATION DISTRIBUTIONS

In this section we compare our measured differential cross sections to various theoretical fragmentation models. We begin with a review of these models.

A. Models of heavy-quark fragmentation

Despite the current impossibility of performing rigorous QCD calculations of the hadronization process, most fragmentation models are, in different ways, inspired by QCD. The one that seems best to describe the experimental data is the Lund model[4,5] which views the fragmentation as a succession of breakings of a QCD string due to the creation, through a tunneling process, of $q\bar{q}$ (or diquark-antidiquark) pairs from the vacuum. After the pioneering work of Field and Feynman,[3] the Lund group produced a widely used Monte Carlo computer program[32] of quark and gluon hadronization. This approach is completely stochastic: amplitude phases and interferences effects are ignored.

A substantially different approach is that of the so-called "shower-cluster" model[6–8] in which the QCD field-theoretical approach is used to generate a shower of quarks and gluons. The current ignorance of the confining process does not allow carrying out this nice approach to its ultimate result. Depending on the models, when the mass of the clusters generated in the QCD shower becomes less than an assigned parameter or when the parton mass is evolved below some minimum value, the showering is stopped and each of the clusters is transformed into a few hadrons either by a completely random, phase-space mechanism or by reverting to the string model fragmentation. Monte Carlo programs are also available for this model, which has the advantage of preserving the quantum-mechanical amplitude of the process, at least in the perturbative regime. At the center-of-mass energies of our experiment the nonperturbative regime essentially dominates the hadronization process. For this reason, and also because of the lack of a closed analytical expression for the fragmentation function, we do not compare this model with our results.

Closed analytical formulas for the fragmentation function were derived in the context of the string model by Anderson *et al.*[5] and Bowler.[45] They are reproduced in Table X, where first we define the scaling variables to be used. Here m_Q is the heavy-quark mass and m_H ($m_{H\perp}$) is the hadron (transverse)[46] mass. According to Bowler's derivation, $B = \Pi/(2\kappa^2)$, where Π is the probability of creating a quark-antiquark pair per unit time and per unit string length, and κ is the energy per unit length, or tension, of the string. Thus B is a parameter with a direct, and possibly fundamental, physical interpretation. We have introduced a factor $(1-x^+)^\beta$ in the Bowler function to take into account radiative corrections. Although they are derived in very different ways, the two expressions differ only by a small logarithmic term in the exponent.

Kartvelishvili *et al.*[47] derived a very different expression for the fragmentation function using the reciprocity rule that states that, for $x \to 1$, the fragmentation function of a heavy quark into a hadron should equal the structure function of that quark in that hadron. Their result is also given in Table X, where α_Q is a quark flavor-dependent parameter.

A basic quantum-mechanical approach was used by Peterson *et al.*[48] A factor $1/\Delta E$ is necessarily present, they argued, in the perturbative amplitude for the transition $Q \to H + q$, where Q is a heavy quark, q a light quark, and H a hadron made of $Q\bar{q}$. Here ΔE is the difference in energy between the initial heavy-quark state and the final state of a hadron plus the remaining light quark. The parameter ϵ_Q is the square of the ratio between the transverse mass of the light quark and the mass of the heavy-quark involved. When taking into account the one-dimensional phase-space factor $1/x$, the formula in Table X results.

Collins and Spiller[49] argued that Petersen's formula, behaving as $(1-x)^2$ for $x \to 1$, disagrees with the reciprocity rule. They have calculated a factor that, taking into account also the transverse motion, restores the agreement with the reciprocity rule and results in the formula shown in Table X, where k_T is the hadron's transverse momentum.

It may be useful to summarize the rationale of the individual factors appearing in the formulas of Table X as follows.

The factor

$$\exp\left[-B\frac{m_{H\perp}^2}{x^+}\right], \tag{14}$$

according to Bowler,[45] expresses the probability of the hadron H to be formed in the string fragmentation process at a time and point such as to give the appropriate value of x^+, the string not having broken before that time. It provides a strong attenuation at low x^+ that may falsely appear as a threshold but is in fact independent of the center-of-mass energy.

The factor $1/x^+$ expresses longitudinal phase space.

The factor $(1-x^+)^\beta$, with $\beta \simeq 1$, approximately takes into account QCD radiative corrections. In other words, because of gluon bremsstrahlung, only a fraction of the primary quark energy is available to the first-rank primary meson. This factor is particularly important in heavy-quark fragmentation for which the corresponding heavy hadron is believed to be always a first-rank hadron.

The Petersen factor is

$$\left[1-\frac{1}{x}-\frac{\epsilon_Q}{(1-x)}\right]^{-2} . \tag{15}$$

It expresses the presence of a typical $(1/\Delta E)^2$ term in the perturbative process $Q \to H + q$. It behaves as $(1-x)^2$ for $x \to 1$, even without a radiative correction factor.

TABLE X. Analytical expressions of the fragmentation functions.

Definition of the scaling variables:

$$x = p/p_{\max}\ ,\quad x^+ = \frac{E+p_\parallel}{E_{\max}+P_{\max}},$$

where E and $p_\parallel$ are the energy and longitudinal momentum of the hadron; $E_{\max}$ and $p_{\max}$ are the maximum values attainable.

Lund symmetric function (Andersson *et al.*):

$$D_Q^H(x^+) = N\frac{(1-x^+)^\beta}{x^+}\exp\left[\frac{-Bm_{H\perp}^2}{x^+}\right].$$

Modified Bowler:

$$D_Q^H(x^+) = N\frac{(1-x^+)^\beta}{x^+}\exp\left\{-Bm_Q^2\left[\frac{m_H^2}{m_Q^2 x^+}-1-\ln\left[\frac{m_H^2}{m_Q^2 x^+}\right]\right]\right\},$$

where $B \equiv (\Pi/2\kappa^2)$.

Kartvelishvili *et al.*: $D_Q^H(x) = Nx^{\alpha_Q}(1-x)$.

Peterson *et al.*:

$$D_Q^H(x) = N\left[x\left[1-\frac{1}{x}-\frac{\epsilon_Q}{(1-x)}\right]^2\right]^{-1},$$

where $\epsilon_Q \equiv m_{q\perp}^2/m_{Q*}^2$.

Collins and Spiller:

$$D_Q^H(x) = N\left[\frac{1-x}{x}+\frac{2-x}{1-x}\epsilon_Q\right](1+x^2)\left[1-\frac{1}{x}-\frac{\epsilon_Q}{1-x}\right]^{-2},$$

where $\epsilon_Q \equiv \left[\frac{\langle k_T^2\rangle}{m_Q^2}\right]$, $\langle k_T^2\rangle = (0.45\ \text{GeV})^2$.

B. Effects of gluon and photon radiation and of charmed-hadron excited states

Two factors serve to complicate the comparison of the theoretical fragmentation functions with data. First, a large fraction of the observed D^0 and D^+ are known to be decay products of D^* and a similar situation may well be true for the D_s and Λ_c. This results in significant softening of the observed spectra relative to those of the hadrons produced directly. Second, QED initial- and final-state radiation as well as QCD gluon radiation contribute to degrading the energy of the initial charm quarks and, as a consequence, of the charmed hadrons.

To minimize the first effect, we limit the direct comparison with the fragmentation functions to the D^{*+} data which, except for a possible small contamination from D^{**} decay,[50] are believed to be primary charm fragmentation products.

QCD radiation is important even at our center-of-mass energy. The most visible and calculable effect is a suppression of the high x spectrum, approximately proportional to $(1-x)$. The fragmentation functions discussed above, with the exception of Petersen's contain a factor $(1-x)^\beta$ and can thus adjust for this radiation. However, the only correct way to take fully into account the QED and QCD corrections and the feed down effect from excited charmed states, is to use a Monte Carlo simulation that incorporates all these features, thus allowing a comparison with the fragmentation distributions of all the observed charmed particles.

C. Comparison with the fully simulated Lund symmetric model

A complete comparison of our data with the Lund symmetric model of string fragmentation[51] can only be done with a full simulation of the model, i.e., using the Lund Monte Carlo procedure[32] which includes the effects of QED and QCD radiation, those of conservation of all quantum numbers, and also other effects typical of the string model.[52,53] We have performed such a comparison using our D^{*+}, D^0, D^+, D_s, and Λ_c fragmentation distribution, while optimizing (as described in more detail in Appendix B) the two parameters β and B of the Lund symmetric fragmentation function (see Table X). An overall normalization factor was determined by comparison with the measured D^{*+} fragmentation distribution. We used the D^{*+} sample because, as already mentioned in Sec. IV C, statistically it is the most accurate, has the least background, and is measured through two different

D^0 decay modes, allowing a check of the systematic errors. The normalization of the D^+ and D^0 distributions are calculated using the known decay branching fractions[36] of those particles. Because of large uncertainty in the values for the decay branching ratios of the D_s and Λ_c, we have treated the normalizations of these two fragmentation distributions as independent parameters.

The optimization resulted in the values

$$\beta = 0.60 \pm 0.10 \pm 0.04 ,$$

$$B = 0.52 \pm 0.05 \pm 0.03 \text{ GeV}^{-2} ,$$

where the first error is statistical and the second, systematic, is due to the uncertainties in the D^0 and D^+ branching fractions and to the possible range of values of one of the parameters in the simulation of the QCD radiative corrections (see Appendix B).

The resulting Monte Carlo fragmentation distributions are shown as the curves in Figs. 10–14. The χ^2 confidence level for the fit is 38%. This shows that the Lund model provides an excellent simultaneous fit to all five distributions using the same values for the two parameters of the Lund symmetric fragmentation function.

Since the Lund Monte Carlo procedure takes into account the QCD radiative corrections, it should correctly predict the fragmentation distribution at any center-of-mass energy if it has the parameters appropriate to reproduce the experimental distribution at one energy. We have tested this using the Lund Monte Carlo procedure, with the parameter values we obtained above from our data, to calculate the predicted D^* fragmentation distribution at a center-of-mass energy ($\sqrt{s} = 30.4$ GeV) that is the average of the PEP and PETRA energies used in Sec. IV C. Figure 18 shows the comparison of this distribution with the one obtained through the evolution equation in that section. The two approaches seem completely equivalent.

The parameters β and B also determine the particle multiplicity in e^+e^- annihilation into hadrons. In fact, as reported in Ref. 32, the JADE Collaboration found empirically that, in order to reproduce the observed multiplicity, the combination $(\beta+0.3)/B$ should have a value of ~ 1.86. This is in agreement with the result of our fit that gives $(\beta+0.3)/B = 1.73 \pm 0.11 \pm 0.06$.

The ratio $B \equiv (\Pi/2\kappa^2)$ of the probability of creating a quark-antiquark pair per unit time and per unit string length to twice the square of the energy per unit length,

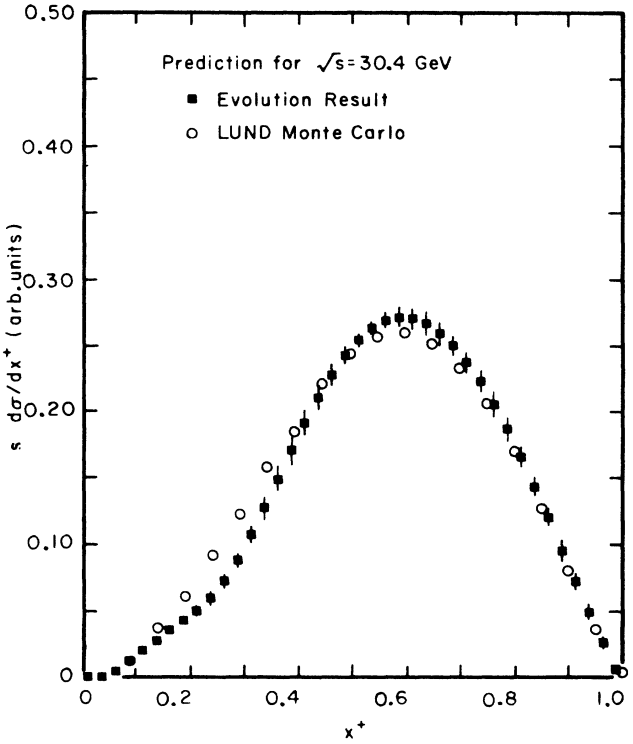

FIG. 18. Comparison of the evolved CLEO D^{*+} fragmentation distribution from Fig. 16 (solid squares) with the predicted distribution from the Lund Monte Carlo procedure for a center-of-mass energy of 30.4 GeV (open circles).

or tension, of the string is a basic, physically meaningful parameter of the string model. Our procedure for determining this parameter takes into account all the details of the model as simulated in the Lund Monte Carlo procedure and is thus more reliable than the value obtained by directly fitting the fragmentation distributions with the analytical formula of the Lund symmetric function described in the next section. Assuming $\kappa \sim 0.2$ GeV$^2 = 1$ GeV/fm (from the slope of the Regge trajectories) we get $\Pi \sim 0.04$ GeV^{-2}.

It should be mentioned that the Lund Monte Carlo simulation does not, at present, produce excited meson states beyond the vector mesons. If a fraction of the D^{*+}'s are decay products of a D^{**}, the softening of the D^{*+} spectrum may affect the value of both β and B.

TABLE XI. Fitted parameters for D^* fragmentation models.

	χ^2/DF	$s\sigma_{\text{tot}}$ (nb GeV^2)
Andersson model:		
$\beta = 1.02 \pm 0.12$, $B = 0.43 \pm 0.07$ GeV^{-2}	7.5/8	71.7±5.4
Bowler model:		
$\beta = 0.95 \pm 0.11$, $B = 0.63 \pm 0.11$ GeV^{-2}	7.1/8	69.7±4.9
Peterson model:		
$\epsilon_Q = (m_q^2 + p_{q\perp}^2)/m_c^2 = 0.156 \pm 0.015$	40.0/10	65.2±3.1
Collins model:		
$\epsilon_Q = \langle k_T^2 \rangle / m_Q^2 = 0.64 \pm 0.14$	6.3/10	76.0±4.4
Kartvelishvili model:		
$\alpha_Q = 1.40 \pm 0.18$	6.0/10	80.7±5.8

D. Analytical fits to the D^{*+} fragmentation distribution

Previous experiments have compared their measured fragmentation distributions directly with the analytical fragmentation functions discussed in Sec. VI B. For reasons of comparison with the other experiments we have therefore also fitted those analytical fragmentation functions directly to our measured D^{*+}-production differential cross section. We have used the Andersson[51] and Bowler[45] functions to fit the x^+ distribution, according to their theoretical derivation. For the Collins,[49] Kartvelishvili,[47] and Peterson[48] functions we have used the distribution in the x variable. This is consistent with their theoretical derivation and it is also a necessity since these functions remain quite large even below the kinematical limit for x^+. The D^{*+} distribution and its fits are shown in Fig. 19. The fitted values of the fragmentation parameters and the resulting value of the total scaling cross section $s\sigma_{\rm tot}$ are tabulated in Table XI.

Not surprisingly, the values for the two parameters β and B of the Lund symmetric function found with this method are considerably different from those obtained in the previous section. The parameter B is thus strongly dependent on the radiative and other corrections[53] present in the Lund Monte Carlo procedure and, in so far as those corrections are correctly handled, only the value $B=0.52\pm0.05\pm0.03$ GeV^{-2}, obtained through the full simulation of the model in the Monte Carlo procedure, should be considered to have physical meaning.[54]

One can see that all the models give a very satisfactory χ^2 except Peterson's. Direct fits of the Peterson function have been quite successful in describing previous results of heavy-quark fragmentation, but the substantially improved accuracy of the current experiment makes the discrepancy quite apparent. The poor fit of the Peterson function is largely due to its $(1-x)^2$ behavior at high x, in strong disagreement with the three highest bins of the experimental distribution. The introduction of a further factor $(1-x)$ to account for the QCD radiative corrections would seem only to worsen the disagreement. We found, however, that use of the Petersen function within the Lund Monte Carlo procedure[55] gives a very good $\chi^2/{\rm DF}=7.8/9$ with $\epsilon_Q=0.076\pm0.009$. This value of ϵ_Q is quite different from the value of 0.156 ± 0.015 obtained by directly fitting the analytical formula to the data, but is in agreement with the theoretically expected value of $\epsilon=(m_q^2+p_{q\perp}^2)/m_c^2\sim0.07$. Apparently, the spectrum-softening string model corrections already mentioned,[53] combined with the hard spectrum given by a small value of ϵ, give a good description of the data. This was previously pointed out by Bethke.[34] Also in this case, we see the danger of attributing physical meaning to the fragmentation function parameters unless a full simulation of the fragmentation process is carried out in a Monte Carlo calculation.

The value of $\epsilon=0.156\pm0.015$ obtained by directly fitting the analytical formula, is in good agreement with our previous result (0.14 ± 0.03) (Ref. 23) as well as with that from the ARGUS group (0.19 ± 0.03) (Ref. 20) at the same center-of-mass energy, and with that of the TASSO (0.18 ± 0.07) (Ref. 16) and the JADE experiment (0.24 ± 0.08) (Ref. 18) at the PETRA energy. However, it is appreciably smaller than the values found by the HRS $(0.41^{+0.10}_{-0.08})$ (Ref. 11) and the DELCO $(0.31^{+0.10}_{-0.08})$ (Ref. 11) Collaborations.

Our value for the parameter ϵ_Q in the Collins fragmentation function is surprisingly much bigger than the one they predict, $(0.45/m_c)^2=0.09$, for $m_c=1.5$ GeV (Ref. 49). Here too we could expect to obtain a smaller value of ϵ_Q if we were to use the Collins function within the Lund Monte Carlo procedure, as was the case for the

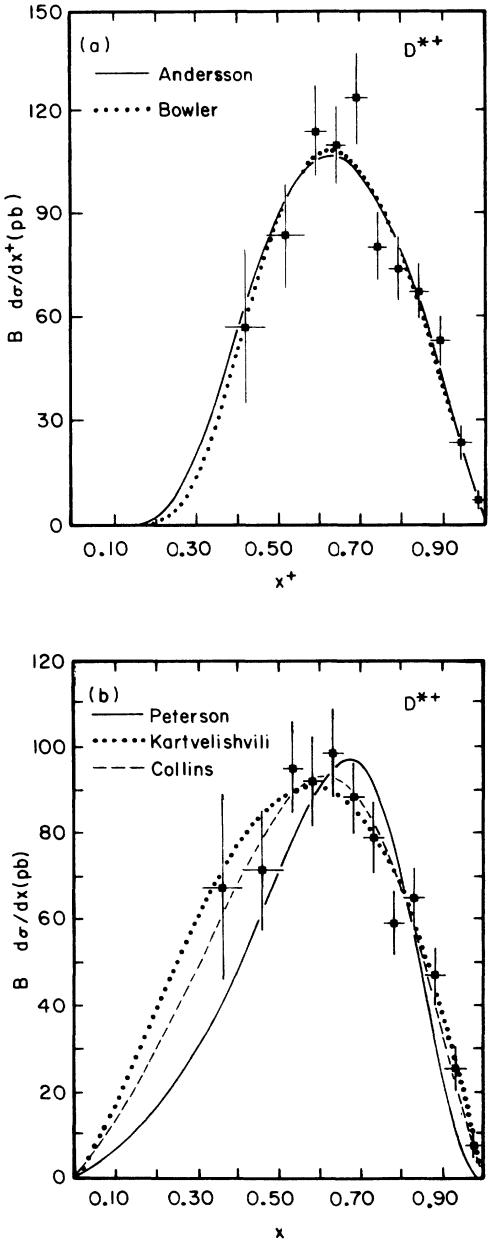

FIG. 19. A fit of the experimental D^{*+} fragmentation distribution to the analytical, theoretical fragmentation functions (Tables X and XI) of (a) Andersson and Bowler and (b) Collins, Kartvelishvili, and Peterson.

Peterson function. We doubt, however, that this is a sufficient explanation for the discrepancy.

The fragmentation of quarks into charmed baryons can be formulated in a similar way to meson formation, with either diquark-pair creation replacing quark-pair creation,[56,57] or modeled as having two independent quark-pair vertices as done by DeGrand.[58] In the latter model, the same value of the Peterson parameter $\epsilon_Q \sim 0.2$ that fits the charmed-meson fragmentation distributions should be used. As shown in Fig. 20, when this is done the DeGrand model disagrees strongly with our Λ_c data [$\chi^2=34$ with six degrees of freedom (DF)]. On the other hand, the diquark model, either through our global fit with the Lund symmetric function in the Lund Monte Carlo procedure (Fig. 14, $\chi^2=6.8$ with seven DF), or through a direct fit with the analytical Peterson fragmentation function (Fig. 20, $\chi^2=3$ with five DF, $\epsilon_Q=0.24\pm0.10$), gives an excellent fit to the data. This confirms our earlier result[25] that the diquark model is a preferable explanation for charmed-baryon fragmentation. However, the Lund symmetric function gives a theoretical distribution slightly harder than the data (Fig. 14).

VII. SUMMARY

Experimental fragmentation distributions for D^{*+}, D^{*0}, D^0, D^+, D_s^+, and Λ_c from e^+e^- annihilations at $\sqrt{s}=10.55$ GeV have been presented. They have been shown to be described very well by the Lund symmetric string fragmentation model, when including the QED and QCD radiative corrections built in the Lund Monte Carlo procedure.

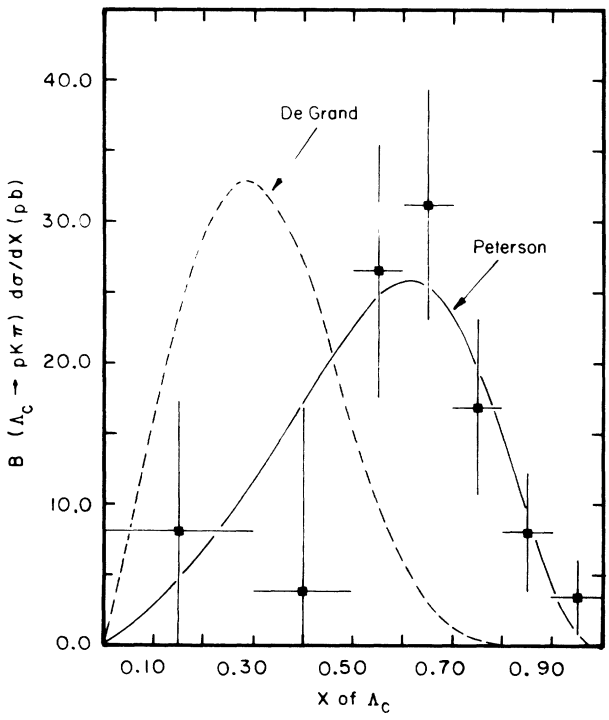

FIG. 20. The experimental Λ_c fragmentation distribution $B\,d\sigma/dx$ compared to the theoretical fragmentation function of DeGrand using a value of the Peterson parameter of $\epsilon=0.2$.

For the ratio of the probability of creating a quark-antiquark pair per unit time and per unit string length to twice the square of the energy per unit length, or tension, of the string, we find $B\equiv(\Pi/2\kappa^2)=0.52\pm0.05\pm0.03$ GeV^{-2}. This measurement should be compared to the value of 0.43 ± 0.07 GeV^{-2} obtained by directly fitting the analytical formula for the Lund fragmentation function to the D^{*+} distribution. We believe that the former result should be used since its determination takes into account all the known features of the string fragmentation model. It implies for the probability of creating a quark-antiquark pair per unit time and per unit string length a value $\Pi\sim0.04$ GeV^{-2}.

A larger discrepancy between the value of the fragmentation parameter obtained through a full simulation of string fragmentation and that obtained by a direct fit of the fragmentation function to the data is found in fitting the Peterson fragmentation function to the D^{*+} data. By the former method we find $\epsilon_Q=0.076\pm0.009$, while direct fitting results in $\epsilon_Q=0.156\pm0.015$. This shows the sensitivity of model parameters to the actual implementation of the full fragmentation scheme, including QCD radiative corrections.

The importance of the QCD corrections is supported by the comparison of our D^{*+} fragmentation distribution with those obtained from experiments at higher center-of-mass energies at PEP and PETRA. The agreement is appreciably improved when we evolve our distribution to the higher energies using the QCD evolution equation.[35] The evolved distribution also agrees with the Lund Monte Carlo prediction when using the parameters that fit our data.

We have measured the probability P_V for a charmed meson to be produced as a vector meson using our measured values of the total D^{*+}, D^{*0}, D^0, and D^+ production cross sections and the known D^0 and D^+ decay branching fractions. Our best estimate of this quantity is $P_V=0.85\pm0.11\pm0.17$. It is to be compared with the naive expectation, based on spin state counting, of $P_V=0.75$ and with the prediction of $P_V=0.63$ by Buchanan and Chun.[44]

Also the branching fraction $B_*\equiv B(D^{*+}\to D^0+\pi^+)$ can be calculated from our measured values of the total D^{*+}, D^{*0}, D^0, and D^+ production cross sections and the known D^0 and D^+ decay branching fractions, obtaining $B_*=0.52\pm0.07\pm0.11$. This result should be compared with the previous results of Goldhaber *et al.*[41] (0.60 ± 0.15), of Coles *et al.*[42] (0.44 ± 0.07), and with the recent preliminary result ($0.55\pm0.02\pm0.06$) of the Mark III Collaboration.[43]

The total (D^0+D^+) production cross section, fully corrected using the D^0 and D^+ decay branching ratios from the Mark III experiment,[36] accounts for $(71\pm6\pm10)\%$ of the expected charmed-particle production cross section if we assume that a $c\bar{c}$ pair is produced in $(37\pm2)\%$ of the e^+e^- annihilations into hadrons. This result is consistent with other experiments.[39]

We have also determined with higher precision than previous experiments[36,20] the ratio of two D^0 branching

fractions:

$$B(D^0\to K^-\pi^+\pi^-\pi^+)/B(D^0\to K^-\pi^+) = 2.12\pm0.16\pm0.09 .$$

ACKNOWLEDGMENTS

We gratefully acknowledge the excellent efforts of the CESR staff which made this work possible. We also gladly acknowledge many useful discussions with Carl Rosenzweig. We are grateful for the use of the Cornell National Supercomputer Facility, which is funded in part by the National Science Foundation, the State of New York and IBM. This work was supported by the National Science Foundation and the U.S. Department of Energy under Contracts Nos. DE-AC02-76ER01428, DE-AC02-76ER03066, DE-AC02-76ER03064, DE-AC02-76ER01545, DE-AC02-76ER05001, and FG05-86-ER40272. Thanks are due from H.K. and R.K. to the Department of Energy Outstanding Junior Investigator program and from K.K. to the Mary Ingraham Bunting Institute for their support.

APPENDIX A: CALCULATION OF B_* AND P_V FROM THE OBSERVED CROSS SECTIONS

We define the following notation:

$P_V \equiv \text{vector}/(\text{pseudoscalar}+\text{vector})$,

i.e., the probability that a meson be a vector meson

$B_* \equiv B(D^{*+}\to D^0\pi^+)$, $B_+ \equiv B(D^+\to K^-\pi^+\pi^+)$,

$B_{02} \equiv B(D^0\to K^-\pi^+)$, $B_{04} \equiv B(D^0\to K^-\pi^+\pi^-\pi^+)$,

$B_0 \equiv B_{02}+B_{04}$,

$N(X) \equiv \sigma(X) \equiv$ total production cross section for particle X ,

$n(X) \equiv B\sigma(X) \equiv$ production cross section for particle X decaying into the observed decay mode .

We obtain the following relations:

$$n(D^{*+}) = N(D^{*+})B_*B_0 , \tag{A1}$$

$$n(D^{*0}) = N(D^{*0})B_{02} , \tag{A2}$$

$$n(D^+) = [N_{\rm dir}(D^+)+N(D^{*+})(1-B_*)]B_+ , \tag{A3}$$

$$n(D^0) = [N_{\rm dir}(D^0)+N(D^{*0}) + B_*N(D^{*+})]B_{02} , \tag{A4}$$

where $N_{\rm dir}(D^+)$ and $N_{\rm dir}(D^0)$ are the numbers of D^+ and D^0 directly produced.

Assuming that $N(D^{*+})=N(D^{*0})$ and that $N_{\rm dir}(D^+)=N_{\rm dir}(D^0)$, one can calculate B_*, P_V, and their product in various ways from the four relations above as different but not independent functions of the measured cross sections and the decay branching ratios. These functions are described below. The best estimates of B_*, P_V, and B_*P_V are the weighted averages of these different functions, using as weights the inverse of the sum of the squares of their statistical and systematic errors. The errors on the weighted averages are calculated using the weighted averages of the partial derivatives of the different functions with respect to the measured cross sections and branching ratios, thus taking into account the correlations among the different functions.

We can calculate the D^{*+} decay branching ratio B_* by taking the ratio of Eqs. (A1) and (A2) and using the equality of the D^{*0}- and D^{*+}-production cross sections:

$$B_* = n(D^{*+}\to(K^-\pi^+)\pi^+)/n(D^{*0}) , \tag{A5}$$

where we have used the D^{*+}-production cross section for D^{*+} with daughter D^0 decaying into $K^-\pi^+$. Equation (A5) gives $B_*=0.55\pm0.07\pm0.11$.

Using the D^{*+} production cross section for D^{*+} with daughter D^0 decaying into $K^-\pi^+\pi^-\pi^+$, the ratio of Eqs. (A1) and (A2) gives

$$B_* = n(D^{*+}\to(K^-\pi^+\pi^-\pi^+)\pi^+)B_{02}/[n(D^{*0})B_+] . \tag{A6}$$

We thus get $B_*=0.49\pm0.07\pm0.13$.

Recalling that $(1-P_V)/P_V$ is the ratio of the number of pseudoscalar to vector mesons and that D^{*0} decays entirely to D^0, Eqs. (A3) and (A4) give, respectively,

$$\frac{n(D^+)}{B_+} = \frac{n(D^{*0})}{B_{02}}\left[\frac{1}{P_V}-B_*\right] , \tag{A7}$$

$$\frac{n(D^0)}{B_{02}} = \frac{n(D^{*0})}{B_{02}}\left[\frac{1}{P_V}+B_*\right] . \tag{A8}$$

Taking the difference of these two equations we obtain the relation

$$B_* = \frac{B_{02}}{2n(D^{*0})}\left[\frac{n(D^0)}{B_{02}}-\frac{n(D^+)}{B_+}\right] , \tag{A9}$$

which gives $B_*=0.49\pm0.10\pm0.12$.

The weighted average of these three measurements gives our best estimate for the D^{*+} decay branching ratio:

$$B_* = 0.52\pm0.07\pm0.11 . \tag{A10}$$

To calculate the product B_*P_V we make the same assumptions used in deriving Eqs. (A7) and (A8), but use the D^{*+} production cross section, to obtain the relations

$$\frac{n(D^+)}{B_+} = \frac{n(D^{*+})}{B_0}\left[\frac{1}{P_VB_*}-1\right] , \tag{A11}$$

$$\frac{n(D^0)}{B_{02}} = \frac{n(D^{*+})}{B_0}\left[\frac{1}{P_VB_*}+1\right] . \tag{A12}$$

Equation (A11) results in $1/(B_*P_V)=2.12\pm0.35\pm0.46$ and Eq. (A12) gives $1/(B_*P_V)=2.31\pm0.21\pm0.25$. The weighted average of these two values is

$1/(B_* P_V)=2.21\pm0.22\pm0.29$, which corresponds to $B_* P_V=0.44\pm0.04\pm0.05$.

Dividing this value of $B_* P_V$ by the value (A10) of B_*, we obtain one estimate of P_V:

$$P_V=0.86\pm0.11\pm0.19 \ . \tag{A13}$$

Another way to calculate P_V is to take the sum of Eqs. (A7) and (A8):

$$\frac{1}{P_V}=\frac{B_{02}}{2n(D^{*0})}\left[\frac{n(D^+)}{B_+}+\frac{n(D^0)}{B_{02}}\right], \tag{A14}$$

which gives $P_V=0.84\pm0.10\pm0.17$. The weighted average of this value and the one in Eq. (A13) gives our final answer of

$$P_V=0.85\pm0.11\pm0.17 \ . \tag{A15}$$

APPENDIX B: OPTIMIZATION OF THE LUND FRAGMENTATION PARAMETERS

Samples of 800 000 $e^+e^-\to c\bar{c}$ events were generated by version 5.2 of the Lund Monte Carlo simulation using the string fragmentation scheme and the Lund symmetric function, and including second-order radiative corrections for QCD and QED. The parameters β and B of the Lund symmetric function (see Table X) were varied.

Since obtaining the χ^2 for each set of values for the two parameters required a separate Monte Carlo run, we minimized the running time by treating the primary hadrons as stable particles except for the excited charmed mesons (D^* and D_s^*) and charmed baryons (Σ_c^*). Hence, Monte Carlo parameters such as the probabilities for vector-meson production of light hadrons $[P(V)/P(V)+P(PS)]=0.50$, for strange-particle production $[P(s)/P(u)=0.29]$, and for baryon production $[P(qq)/P(q)=0.068]$, are largely irrelevant to the fit.

The Monte Carlo (MC) simulated D^{*+} fragmentation distribution was normalized to the corresponding data and the normalization factor so obtained, together with the parameter P_V and the D^{*+}, D^0, and D^+ branching ratios, was used to normalize the D^0 and D^+ distributions.

We use the same notation as in Appendix A, and in addition we define $M^*, M^+, M^0 \equiv$ number of D^{*+}, D^+, D^0 generated in the Monte Carlo.

The normalization factor r^* for the D^{*+} is calculated from a direct comparison of the total number of entries in the data and Monte Carlo fragmentation distributions, for the region of x^+ in which data are available:

$$r^*=\frac{n(D^{*+})}{M^*}=\frac{N(D^{*+})B_* B_0}{M^*} \ . \tag{B1}$$

The normalization factors for the D^+ and D^0 (r^+ and r^0) can then be easily calculated by recalling that D^{*0} decays entirely to D^0 and assuming that $N(D^{*+})=N(D^{*0})$:

$$r^+=\frac{n(D^+)}{M^+}=\frac{\frac{n(D^{*+})}{B_* B_0}\left[\frac{1-P_V}{P_V}+(1-B_*)\right]B_+}{M^+}$$
$$=\frac{n(D^{*+})}{M^+}\frac{B_+}{B_0}\left[\frac{1}{B_* P_V}-1\right], \tag{B2}$$

$$r^0=\frac{n(D^0)}{M^0}=\frac{n(D^{*+})}{M^0}\frac{B_{02}}{B_0}\left[\frac{1}{B_* P_V}-1\right] . \tag{B3}$$

For P_V and B_* we used the values determined in this experiment (Sec. V), while we used the values in Ref. 36 for the D^0 and D^+ decay branching ratios. The D_s and Λ_c MC x^+ distributions were directly normalized to the corresponding distributions in the data. The χ^2 for each Monte Carlo run is obtained by comparing bin by bin the MC x^+ distributions for the D^{*+}, D^0, D^+, D_s, and Λ_c thus normalized, to the corresponding data distributions.

After a random search for an approximately optimum set of values for the two parameters, four MC samples were generated, varying one parameter at a time by plus or minus a suitable step. If any one of the four χ^2 values was smaller than the central one, the corresponding parameter values were chosen as the new optimum set and the procedure repeated with smaller steps until the central value remained the best. At that stage the optimum value of the parameters was calculated by minimizing the χ^2 using a simple parabolic approximation independently for each parameter. One MC sample with the optimum values of the parameters, four MC samples varying one parameter at a time, and four MC samples changing two parameters at a time were generated. The χ^2's for these nine samples allowed the calculation of the Hessian (the second-derivative matrix) of the χ^2 as a function of the two parameters. Inversion of the Hessian provided the variance matrix and hence the statistical errors. The optimum values and their errors are

$$\beta=0.60\pm0.08 \ , \quad B=0.52\pm0.03 \ \text{GeV}^{-2} \ . \tag{B4}$$

The total χ^2 for the five fragmentation distributions was 45.3 with 43 degrees of freedom, giving a confidence level of 38%.

Since the parameters P_V and B_* are calculated from the same data sample, their errors contribute to the statistical error in β and B. The main effect of P_V and B_* is to determine the relative amount of D^{*+}'s with respect to D^+'s and D^0's; however, they also affect the shape of the momentum distribution of the latter two, because of the lower momentum of the D's that are decay products of D^*'s. We have conducted an independent optimization varying, besides β and B, also P_V and β_*. This procedure gave, as statistical errors

$$\sigma_\beta=0.10 \ , \quad \sigma_B=0.05 \ \text{GeV}^{-2} \ , \tag{B5}$$

which, taking into account the variability of P_V and B_*, give a better estimate of the errors than those in Eq. (B4).

The procedure just described neglects the error due to statistical fluctuations in $n(D^{*+})$, the observed number of D^{*+}. We have therefore repeated the fitting of the two parameters by changing the value of $n(D^{*+})$ by

$[n(D^{*+})]^{1/2}$. The differences between the resulting fitted parameters and the previous set give us the following contributions to the statistical errors:

$$\sigma_\beta = 0.025 \ , \quad \sigma_B = 0.020 \ \text{GeV}^{-2} \ .$$

We have combined these errors quadratically with the ones in (B5) to give the statistical errors quoted in the text.

Also, the D^0 and D^+ decay branching fractions affect the normalization of the respective fragmentation distributions. We used the errors due to the fluctuations in $n(D^{*+})$ found above to estimate the systematic uncertainty due to the errors in these branching fractions. We obtain

$$\sigma_\beta = 0.039 \ , \quad \sigma_B = 0.032 \ \text{GeV}^{-2} \ .$$

We notice, however, that the branching fractions used all come from the same experiment[36] and appear in ratios in the expressions for the normalization factors above; if the errors quoted in Ref. 36 were correlated, the errors above would be overestimated.

Estimating the systematic errors in a model-dependent calculation is fairly arbitrary. We are, however, aware of the effect of a parameter used in handling gluon bremsstrahlung: $y_{\min} = (m_{ij}/s)_{\min}$, which is the scaled minimum invariant mass between partons i and j for the two partons not to merge into one. It influences the initial four-momentum of the charm quarks and hence the charmed-particle spectrum. We have used the default value of 0.02, but, following the suggestion of Bethke,[34] we have also produced the optimization using 0.04. The half differences between the two results are

$$\sigma_\beta = 0.004 \ , \quad \sigma_B = 0.008 \ \text{GeV}^{-2} \ .$$

We have combined quadratically the two systematic errors above to give the systematic error shown in the main text.

[1] T. Appelquist and H. D. Politzer, Phys. Rev. D **12**, 1404 (1975); E. C. Poggio *et al.*, *ibid.* **13**, 1958 (1976); M. Dine and J. Sapirstein, Phys. Rev. Lett. **43**, 668 (1979); K. G. Chetyrkin *et al.*, Phys. Lett. **85B**, 277 (1979); W. Celmaster and R. J. Gonsalves, Phys. Rev. Lett. **44**, 560 (1979).

[2] C. Bacci *et al.*, Phys. Lett. **86B**, 234 (1979); J. L. Siegrist *et al.*, Phys. Rev. D **26**, 969 (1982); Particle Data Group, M. Aguilar-Benitez *et al.*, Phys. Lett. **170B**, 1 (1986).

[3] R. D. Field and R. P. Feynman, Nucl. Phys. **B136**, 1 (1978).

[4] X. Artru and G. Mennessier, Nucl. Phys. **B70**, 93 (1974).

[5] B. Andersson *et al.*, Phys. Rep. **97**, 33 (1983).

[6] R. D. Field and S. Wolfram, Nucl. Phys. **B213**, 65 (1983).

[7] R. B. Webber, Nucl. Phys. **B238**, 492 (1984).

[8] T. D. Gottschalk, Nucl. Phys. **B214**, 201 (1983); T. D. Gottschalk and D. A. Morris, *ibid.* **B288**, 729 (1987).

[9] P. Soding and G. Wolf, Annu. Rev. Nucl. Part. Sci. **32**, 231 (1981).

[10] Mark II Collaboration, J. M. Yelton *et al.*, Phys. Rev. Lett. **49**, 430 (1982).

[11] HRS Collaboration, M. Derrick *et al.*, Phys. Rev. Lett. **53**, 1971 (1984).

[12] DELCO Collaboration, H. Yamamoto *et al.*, Phys. Rev. Lett. **54**, 522 (1985).

[13] HRS Collaboration, M. Derrick *et al.*, Phys. Lett. **146B**, 261 (1984).

[14] TPC/Two-Gamma Collaboration, H. Aihara *et al.*, Phys. Rev. D **34**, 1945 (1986).

[15] HRS Collaboration, S. Abachi *et al.*, in *Proceedings of the XXIII International Conference on High Energy Physics*, Berkeley, California, 1986, edited by S. C. Loken (World Scientific, Singapore, 1987).

[16] TASSO Collaboration, M. Althoff *et al.*, Phys. Lett. **126B**, 493 (1983).

[17] TASSO Collaboration, M. Althoff *et al.*, Phys. Lett. **136B**, 139 (1984).

[18] JADE Collaboration, W. Bartel *et al.*, Phys. Lett. **146B**, 121 (1984).

[19] JADE Collaboration, W. Bartel *et al.*, Phys. Lett. **161B**, 197 (1985).

[20] ARGUS Collaboration, H. Albrecht *et al.*, Phys. Lett. **150B**, 235 (1985); **153B**, 343 (1985).

[21] ARGUS Collaboration, H. Albrecht *et al.*, in *Proceedings of the XXIII International Conference on High Energy Physics* (Ref. 15).

[22] ARGUS Collaboration, R. S. Orr, in *Proceedings of the International Europhysics Conference on High Energy Physics*, Bari, Italy, 1985, edited by L. Nitti and G. Preparata (Laterza, Bari, 1985), p. 517.

[23] CLEO Collaboration, C. Bebek *et al.*, Phys. Rev. Lett. **49**, 610 (1982); P. Avery *et al.*, *ibid.* **51**, 1139 (1983).

[24] CLEO Collaboration, A. Chen *et al.*, Phys. Rev. Lett. **51**, 634 (1983).

[25] CLEO Collaboration, T. Bowcock *et al.*, Phys. Rev. Lett. **55**, 923 (1985).

[26] CLEO Collaboration, D. Andrews *et al.*, Nucl. Instrum. Methods **211**, 47 (1983).

[27] CLEO Collaboration, S. Behrends *et al.*, Phys. Rev. D **31**, 2161 (1985).

[28] CLEO II Collaboration, Cornell University Report No. CLNS 85/634, 1985 (unpublished).

[29] M. M. Ito, Ph.D. dissertation, Cornell University, 1986.

[30] Note that we do not use the lower sideband to avoid contamination present from $D^0 \to K\pi(\pi^0)$, where the π^0 is unobserved and the $K\pi$ invariant mass therefore falls slighty below the true D mass.

[31] Particle Data Group, M. Aguilar-Benitez *et al.*, Phys. Lett. **170B**, 1 (1986).

[32] T. Sjostrand, Comput. Phys. Commun. **27**, 243 (1982); **28**, 239 (1983); **39**, 347 (1986).

[33] In Figs. 10 and 15 we also show an upper limit to the cross section for D^{*+} production in the interval $0.20 < x^+ < 0.43$ derived, as explained in Sec. III C, assuming equal charged- and neutral-D^* production and no direct D^0 production. Taking our measured D^0 visible cross section

$$B\,\sigma(D^0, 0.0 < x < 0.30) = 5.7 \pm 3.8 \ \text{pb}$$

and the decay branching fractions listed in Sec. IV D, we obtain $B\,d\sigma(D^{*+})/dx^+ = 29 \pm 20$ pb in the interval

$0.20 < x^+ < 0.43$. The statistical uncertainty in the measurement dominates over the uncertainty in the rate of direct D^0 production. This point was not used in any of the fits described later.

[34]S. Bethke, Z. Phys. C **29**, 175 (1985).

[35]Guido Altarelli, Phys. Rep. **81**, 1 (1982).

[36]Mark III Collaboration, J. Adler *et al.*, Phys. Rev. Lett. **60**, 89 (1988).

[37]CLEO Collaboration, R. Giles *et al.*, Phys. Rev. D **29**, 1285 (1984).

[38]In D. Bortoletto *et al.*, Phys. Rev. D **35**, 19 (1987), we reported a result that used the D decay branching fractions in Ref. 59.

[39]See Ref. 11. Their result was multiplied by 1.3 to take into account the most recent D decay branching fractions. See Refs. 36 and 40.

[40]Mark II Collaboration, R. H. Schindler *et al.*, Phys. Rev. D **24**, 78 (1981).

[41]Mark I Collaboration, G. Goldhaber *et al.*, Phys. Lett. **69B**, 503 (1977).

[42]Mark II Collaboration, M. W. Coles *et al.*, Phys. Rev. D **26**, 2190 (1982).

[43]Mark III Collaboration, D. Hitlin, in Proceedings of the International Symposium on Lepton and Photon Interactions at High Energies, Hamburg, 1987 (unpublished).

[44]C. D. Buchanan and S. B. Chun, Phys. Rev. Lett. **59**, 1997 (1987).

[45]M. G. Bowler, Z. Phys. C **11**, 169 (1981); **22**, 155 (1984).

[46]Here, and in the following, "transverse" means transverse with respect to the string direction. A transverse mass $m_\perp = \sqrt{m^2 + p_T^2}$ is an effective mass with respect to the essentially one-dimensional string fragmentation model.

[47]V. G. Kartvelishvili *et al.*, Phys. Lett. **78B**, 615 (1978); Yad Fiz. **38**, 1563 (1983) [Sov. J. Nucl. Phys. **38**, 952 (1983)].

[48]C. Peterson *et al.*, Phys. Rev. D **27**, 105 (1983).

[49]P. Collins and T. Spiller, J. Phys. G **11**, 1289 (1985).

[50]ARGUS Collaboration, H. Albrecht *et al.*, Phys. Rev. Lett. **56**, 549 (1986); in *Proceedings of the XXIII International Conference on High Energy Physics* (Ref. 15), p. 1564; CLEO Collaboration, in Proceedings of the International Symposium on Lepton and Photon Interactions at High Energies, Hamburg, 1987 (unpublished).

[51]B. Andersson, G. Gustafson, and B. Soderberg, Z. Phys. C **20**, 317 (1983).

[52]We have used version 5.2 of the Lund Monte Carlo program. QED and QCD radiation up to second order were allowed, with $\Lambda = 0.5$ GeV and the minimum scaled invariant mass squared between two partons $y = 0.02$ (the Lund default values).

[53]According to the Lund string model, Ref. 5, quark-antiquark pairs are produced through a tunneling mechanism. Because of the (transverse) mass of the pair, the model requires that the string has stretched enough to provide the energy for the pair. This, in turn, has the major effect of softening the high-momentum end of the fragmentation distribution.

[54]As a check we fitted the optimized Monte Carlo simulation at the D^{*+} distribution with the analytical formula for the Lund symmetric function (Table X; we obtained $\beta = 1.070 \pm 0.003$ and $B = 0.435 \pm 0.001$ GeV^{-2}, which are as expected very close to the values obtained by directly fitting the data, since the Monte Carlo simulation accurately reproduces the data.

[55]The Lund Monte Carlo program, Ref. 32, allows the use of several fragmentation functions, besides the Lund symmetric one.

[56]B. Andersson *et al.*, Phys. Scr. **32**, 574 (1985).

[57]S. Fredricsson *et al.*, Phys. Rev. Lett. **51**, 2179 (1983).

[58]T. A. DeGrand, Phys. Rev. D **25**, 3928 (1982).

[59]Mark III Collaboration, R. M. Baltrusaitis *et al.*, Phys. Rev. Lett. **56**, 2140 (1986).